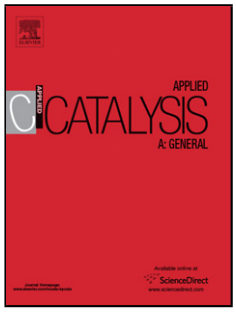

Methane conversion to ethylene over GaN catalysts. Effect of catalyst nitridation

Kanchan Dutta, Vishnu Chaudhari, Chao-Jun Li, Jan Kopyscinski

PII: S0926-860X(20)30023-5

DOI: https://doi.org/10.1016/j.apcata.2020.117430

Reference: APCATA 117430

To appear in: *Applied Catalysis A, General*

Received Date: 18 November 2019

Revised Date: 11 January 2020

Accepted Date: 21 January 2020

Please cite this article as: { doi: https://doi.org/

Revised manuscript No.: APCATA-D-19-02293R1

Methane conversion to ethylene over GaN catalysts. Effect of catalyst nitridation.

Kanchan Dutta[1], Vishnu Chaudhari[1], Chao-Jun Li[2], Jan Kopyscinski[1]*

[1] Department of Chemical Engineering, McGill University,

3610 University Street, Montreal, Quebec H3A 0C5, Canada

[2] Department of Chemistry, McGill University

801 Sherbrooke Street West, Montreal, QC H3A 0B8

* To whom all correspondence should be addressed:

Tel.: +1 514 398 4276

jan.kopyscinski@mcgill.ca

Graphical Abstract

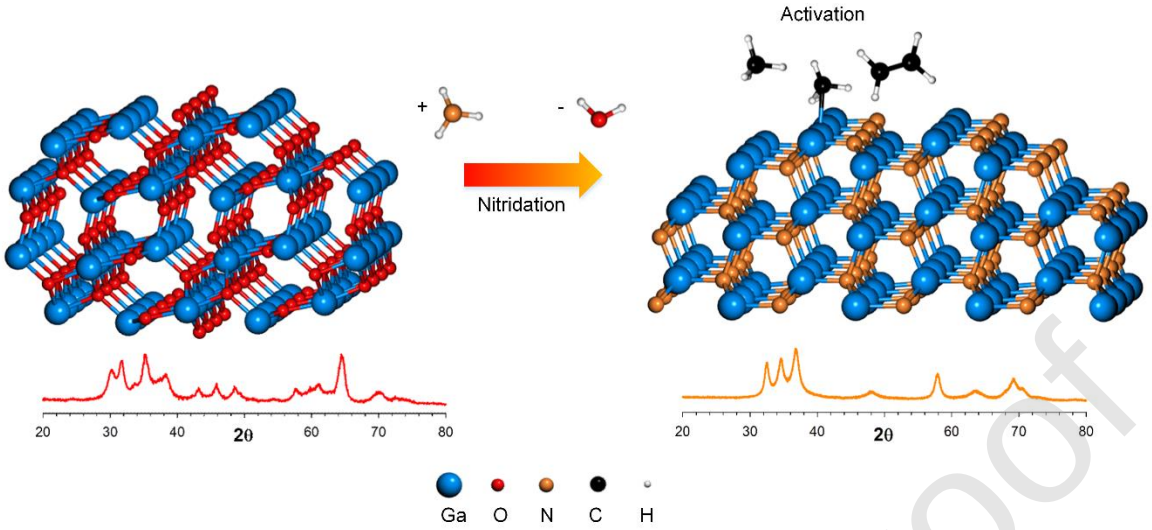

Highlights

- Optimum nitridation temperature for the supported GaN/SBA15 catalyst is 700 °C.
- Nitridation improved atomic economy of CH_4 conversion.
- GaN/SBA15 is more stable and has a lower coke formation than unsupported GaN.
- C_2H_4 selectivity over GaN/SBA15 was 70% and coke selectivity was <30%.
- Ga_2O_3 produced CO_x and H_2O reducing C_2H_4 selectivity below 60% over Ga_2O_3/SBA15.

Abstract

Vast availability of natural and shale gases makes methane a reliable source for synthesizing valuable chemical building blocks such as ethylene. A new stable supported GaN/SBA15 catalyst from an emerging class of nitride catalysts was reported for the direct non-oxidative methane coupling to ethylene. The effect of nitridation on the catalyst properties and activity was investigated. The optimum nitridation temperatures were 700 °C and 750 °C for the GaN/SBA15 and the unsupported GaN catalyst, respectively. Supported catalysts were more stable and had 5-10 times higher product (ethylene) formation rates per gram of gallium than the unsupported catalysts due to the higher surface area (>320 vs. <20 m^2 g^{-1}) and Ga-dispersion inside the pores. Compared to the oxide precursors, the nitrides exhibited a higher atom conversion efficiency for the CH_4 carbon leading to higher ethylene selectivity (71% for GaN/SBA15, <58% for Ga_2O_3/SBA15) and lower coke selectivity (27% for GaN/SBA15, 40% for Ga_2O_3/SBA15).

Keywords: ethylene; direct nonoxidative methane conversion; gallium nitride catalyst; nitridation; SBA-15; catalyst synthesis and characterization.

1 Introduction

The base chemicals for the petrochemical industry like olefins (ethylene, propylene, butadiene) and aromatics (benzene, toluene, and xylenes) are currently derived from oil and natural gas. Estimated to be the world's most widely used petrochemical in terms of production volume,

ethylene is the key building block for polyethylene (50%), ethylene oxide (10%) and its derivatives such as ethylene glycol [1]. It is also used to produce vinyl acetate, polyvinyl chloride, polyester fiber and film, and a range of alcohols and solvents. An estimated 60% of total US ethylene production capacity uses liquefied natural gas, with a further 38% derived using naphtha. In 2018, ethylene accounted for 59% of the petrochemical industry revenue in Canada [2], while aromatic hydrocarbons accounted for 38% of revenues in the United States (2017) [1].

Methane (natural gas, shale gas) is considered to be a reliable source for the petrochemical industry. Methane activation and conversion to value-added chemicals are of great interest not only from the fundamental research perspective but also in terms of industrial application as it offers a potential for an alternative route to produce chemicals. Currently, natural gas is converted via the syngas route (indirect and oxidative) to methanol and its derivatives. This conventional syngas route has low efficiency, high capital cost, and associated greenhouse gas emissions. Direct oxidative coupling of methane is another way [3]. However, a significant amount of CO, CO_2, and H_2O are produced, which lowers the product selectivity.

Direct non-oxidative conversion of methane to olefins and aromatics is an alternative and theoretically a very efficient conversion route [4]. However, methane has a very stable C-H bond, which is very difficult to activate under non-oxidative conditions [5]. The review articles from Ma et al.[4], Spivey and Hutchings [6], and Karakaya and Kee [3] summarize the research work that

has been conducted with emphasis on metal-modified zeolites. Metals such as Mo, Zn, W, Re, Cu, Mn, Ni, and Cr have been investigated. Molybdenum-containing zeolites exhibited the highest activity in terms of methane conversion (3-16%) with benzene (50-75%) as the main product [5]. It is hypothesized that an active species on the catalyst surface (i.e., CH_x) is formed, which further dimerizes to produce ethylene. Finally, ethylene is oligomerized and cyclized on the zeolite to form aromatics [4]. A combination of benzene and the active species like CH_2 and CH_3 can form toluene. Two phenyl species (active aryl rings) can form naphthalene [7,8]. Further combination of phenyl species can lead to the formation of polynuclear aromatic compounds (i.e., coke) that deactivates the catalysts, which is the main drawback of this reaction. Adding promoters such as transition metals in Period 4 (Fe, Co, Ni, and Cr) and metals in Group 13 (Ga and Al) show the best improvement in terms of methane conversion, product selectivity, and catalyst stability [4]. It has been shown that Ga containing zeolites are highly active for the dehydrogenation of light alkane [9,10]. But the nature of the active gallium species as well as the gallium alkane intermediates is still under debate. Recently, Dumesic's group developed PtSn-zeolite catalysts that achieved high ethylene selectivities (70-90% at 700 °C, coke not included); yet coking was still a huge problem [11]. They obtained methane conversions (in terms of fraction converted to the products) less than 0.5%, typically 0.25% at 700 °C. Xiao and Varma [12] used bimetallic PtBi-zeolite catalysts and reported ethane (C_2H_6) selectivity of 90% (coke not included) at 700 °C, with methane conversion between 1-5%. However, they had 40-50% coke selectivity with up to

10% ethylene (C_2H_4) selectivity on 1% Pt-0.2% Bi catalyst at 650 °C and 0.1 atm CH_4 partial pressure. They suggested that carbon deposition occurs during the initial activation period. Bajec et al. [13] used Fe/HZSM- 5, Mo/HZSM- 5, and Fe–Mo/HZSM- 5 catalysts for methane activation and coupling to ethane and ethylene. They obtained 1-6% methane conversion, up to 50% ethylene selectivity and 11-35 wt% coke. Their reaction conditions were T = 700 °C, WHSV = 2 h^{-1}, p_{tot} = 1.5 bar. Sheng et al. [14] used a less acidic boron-based [B]ZSM-5 catalyst for methane activation and obtained 90% ethylene selectivity (gas phase) with less than 1% methane conversion at 700 °C with an average rate of 0.3 $mmol_{CH4}$ h^{-1} g_{cat}^{-1}. Low acidity of the support produced more ethylene than benzene and lower coke. Guo et al. [15] synthesized single iron sites embedded in a silica matrix. They reported minimum carbon deposition, maximum ethylene selectivity of 48%, and maximum methane conversion of 48% at 1090 °C.

Almost all the catalysts studied so far were bifunctional precious metals and metal oxides. Our manuscript focuses on metal nitrides, which are gaining interests as heterogeneous catalysts [16]. Nitride catalysts have been used for ammonia synthesis (Co, Mo, Ru nitrides), ammonia decomposition to obtain CO_2 free H_2 (Ru nitride), and for hydrotreating process (Mo nitride) [16]. Nitrides of Si, B have also been used as catalysts support. Compared to the conventional alumina and silica supports, the nitrides can have greater thermal conductivity, increased inertness, modified basicity, and enhanced hydrophobicity [16]. Gallium nitride, a material used in the semiconductor industry, was tested for the first time for methane activation in a batch reactor [17].

The tests were carried out under Ultraviolet (UV) irradiation at room temperature, and also under thermocatalytic conditions at 450 °C and 5-8 h residence time [18,19]. They demonstrated a high selectivity for benzene (S_{C6H6} = 97% under UV and S_{C6H6} = 89.8%, at 450 °C, respectively). However, due to low temperature and thermodynamic limitations, the methane conversion was less than 0.5%. Higher temperatures (>650 °C) and continuous operations are necessary for achieving larger methane conversion [20]. In the optoelectronics and semiconductor industry, GaN is often synthesized in the form of nanostructures (nanotubes, nanowires, and nanorods) through various procedures such as arc discharge, laser ablation, chemical vapor deposition, plasma-assisted molecular beam epitaxy, and metal-organic vapor phase epitaxy. In most of these procedures, NH_3 at high temperature (nitridation) is used to produce GaN nanostructures from gallium precursors. Some of these methods might not be applicable for the preparation of the catalysts that require a large surface area and well-distributed active sites.

In this work, unsupported catalysts were synthesized, and for the first time, supported gallium nitride catalysts were synthesized, and the effect of the nitridation conditions on the direct non-oxidative methane conversion to value-added chemicals were investigated under flow conditions.

2 Experimental Section

2.1 Catalyst preparation

Two types of catalysts were synthesized; one group was unsupported GaN, the second one was GaN supported on SBA-15 with Ga target loading of 16 wt%. Unsupported catalysts were prepared by the Evaporation Induced Self Assembly (EISA) technique adapted from Chaudhari et al. [21]. Around 1 g of triblock copolymer (Pluronic P-123, Sigma Aldrich) was dissolved in 16 mL of pure anhydrous ethanol (Greenfield Global Inc.) until a homogeneous solution was obtained. This was followed by the addition of 1.7 mL of nitric acid (67-70 wt%, Fisher Scientific) and stirring for complete mixing with the acid. Another solution was prepared in 5 mL DI-water and 5 mL of ethanol with 4.5 g of dry gallium (III) nitrate hydrate powder (99.9998 wt% trace metal basis, ACROS Organic, Thermo Fisher Scientific). DI-water was used to get a homogeneous solution as the nitrate is only slightly soluble in ethanol. The hygroscopic nitrate was always stored under dry inert gas (Ar with < 5 ppm moisture, Praxair) desiccator to prevent moisture absorption. The nitrate bottle was also flushed with Ar after every use. This ensured that the weight of the nitrate was consistent and not influenced by absorbed moisture. The copolymer solution was then added to the gallium precursor solution and stirred for 5 h at 600 rpm at room temperature. The homogeneous, colorless mixture was kept inside a drying oven at 60 °C for 48 h. Thereafter, the dried copolymer-gallium mixture was calcined at 650 °C for 6 h at a heating rate of 1 °C min^{-1} in which the copolymer was burned, and the gallium-precursor was converted to Ga_2O_3. Before

nitridation, the catalysts were dried for 4.5 h in Ar (99.999%, MEGS Specialty Gases, 15-20 mL_N min^{-1}) at 300 °C with a heating rate of 1 °C min^{-1} (subscript *N* denotes normal condition with T = 0 °C and 1 bar). The nitridation was carried out in a fixed bed reactor with anhydrous ammonia (NH_3, 99.99%, MEGS Specialty Gases, 20 mL_N min^{-1}) flowing top-down through the catalyst bed (around 1 g). A quartz tube (9 mm OD × 7 mm ID × 275 mm long) with a 15-40 µ frit at one end was used as the reactor inside a vertical tube furnace (Mellen Company). At the reactor outlet, the gas was mixed and diluted with Ar. A slipstream was analyzed via mass spectrometry (Pfeiffer Omnistar GSD 301 O1), while the rest was sent through a 10 L hydrochloric acid bubbler (36.5–38 wt%, Fisher Scientific) to absorb unreacted ammonia. Nitridation was carried out at five nitridation temperatures (600, 650, 700, 750 and 800 °C at a heating rate of 1.5 °C min^{-1} and 24 h NH_3 exposure from the start of heating to cool down), and ammonia exposure time (3-9 h at 750 °C at a heating rate of 1.5 °C min^{-1}). After cooling to room temperature under the NH_3 atmosphere, the reactor was purged with Ar, and the catalyst sample was stored for further use under inert gas in a desiccator.

Supported gallium catalysts were prepared as follows. Ordered mesoporous silica (SBA-15) was synthesized as described in Zhao et al. [22]. Around 4 g of triblock copolymer (Pluronic P-123, Sigma Aldrich) was dissolved by stirring (600 rpm for 5 h) in 95 mL of deionized water until a homogeneous solution was obtained. To this solution, 4 mL of hydrochloric acid was added and stirred for about 15 min at a temperature of 38.5 °C. Then 9.5 mL of tetraethoxysilane (TEOS,

99.9%, Alfa Aesar) was added. The resulting mixture was stirred at 600 rpm for an additional 24 h at 38.5 °C for completing TEOS hydrolysis and precipitation of silica. The above mixture was placed inside a closed polypropylene digestion DigiTUBEs (SCP science) and kept inside an oven at 100 °C for 48 h for hydrothermal treatment. After cooling down, the white powder was separated by filtration and washed with deionized water several times, followed by overnight drying at 60 °C. Finally, SBA-15 was obtained by calcining the dried solid at 550 °C for 5 h at a heating rate of 1 °C min^{-1}.

Supported catalysts were synthesized by incipient wetness impregnation of SBA-15 with gallium containing precursor. Typically, 1 g of SBA-15 was impregnated with 1 g of gallium (III) nitrate hydrate in 4.5 mL aqueous solution. The almost wet solid was left for 24 h at room temperature followed by drying overnight at 70 °C. The dried solid was then calcined at 550 °C for 5 h at a heating rate of 1 °C min^{-1} to produce gallium oxide inside SBA-15. Nitridation of supported catalysts were carried out in the same manner as described above for the unsupported catalysts. Due to the small bulk density, around 200 mg supported gallium oxide (Ga_2O_3/SBA15) was nitridated at temperatures of 650, 700, 750, and 800 °C. Finally, the supported catalysts were stored in Ar filled vials inside the desiccator.

The produced unsupported catalysts were named Ga_2O_3, GaN-750, or GaN-750-03, referring to the calcined and nitridated samples, respectively. In detail, for GaN-750, the 750 denotes the

nitridation temperature in degree Celsius (°C) with a total NH_3 exposure of 24 h, while for GaN-750-03, the 03 refers to the nitridation time in hours (e.g., 3, 6 or 9 h). The produced supported catalysts were named Ga_2O_3/SBA15 and GaN/SBA15-750, referring to the calcined and nitridated samples, respectively. In detail, for GaN/SBA15-750, the 750 denotes the nitridation temperature in degree Celsius (°C). N-SBA15-800 refers to a nitridated SBA-15 (without Ga_2O_3) with a nitridation temperature of 800 °C.

2.2 Catalyst characterization

The gallium content in the supported catalysts was determined using Inductively Coupled Plasma - Optical Emission Spectroscopy (ICP-OES, iCAP 6500 dual view Thermo Scientific). The supported catalyst was fused with twice the amount (by weight) of lithium tetraborate (SCP science) in a 9 mL graphite crucible (SCP science). The fusion was carried out in a muffle furnace ramping to 950 °C, where it was held for 30 min. A glassy bead was obtained after cooling down, and the fusion flux was carried out in triplicate. Two different solutions were prepared from the bead; one in 10% HNO_3 (trace metal grade) and another one in 3:1 HCl to HNO_3 concentrated solution (aqua regia). These solutions were digested in polypropylene DigiTUBEs (SCP science) at 95 °C for 2 h until the bead was completely dissolved. After cooling down, the solutions were filtered through 45 µ filter and diluted appropriately for ICP analysis. Unsupported catalysts were either GaN or Ga_2O_3 or a mix of both, and no other metals were present in them. Gallium content in unsupported catalysts can be calculated directly without ICP.

The total nitrogen content of unsupported gallium nitride catalysts was determined by Shimadzu TOC-Vcph with TNM–1 Total Nitrogen Module. Prior to the analysis, around 25-50 mg of the sample was dissolved in 6M hydrochloric acid (HCl) overnight at 80 °C. The gallium nitride was converted to gallium chloride and ammonium chloride, while gallium oxide was converted to gallium chloride and water, as shown in Eqs. (1) and (2), respectively.

$$GaN\ (s) + 4\ HCl\ (aq.) \rightarrow GaCl_3(aq.) + NH_4Cl\ (aq.) \quad (1)$$

$$Ga_2O_3\ (s) + 6\ HCl\ (aq.) \rightarrow 2\ GaCl_3\ (aq.) + 3\ H_2O \quad (2)$$

The homogenous and clear solution was cooled down, diluted with deionized water to adjust the pH between 2–3. The diluted solution was analyzed for the total nitrogen content. The instrument was always calibrated before the analysis using ammonium standard (Sigma Aldrich) containing 1000 mg L^{-1} of N as NH_4^+ in water. The pH of the calibration solutions was adjusted between 2–3 by using HCl. Ga_2O_3 conversion ($X_{Ga_2O_3}$) was calculated based on equation 3 below.

$$X_{Ga_2O_3} = \frac{n^0_{Ga_2O_3} - n_{Ga_2O_3}}{n^0_{Ga_2O_3}} \quad (3)$$

Where, $n^0_{Ga_2O_3} = \frac{(1 - n_N \cdot M_{GaN})}{M_{Ga_2O_3}} + \frac{n_N}{2}$ and $n_{Ga_2O_3} = \frac{(1 - n_N \cdot M_{GaN})}{M_{Ga_2O_3}}$, are mol of Ga_2O_3 before and after nitridation (unconverted), respectively. n_N denotes the mol of nitrogen in 1 g of unsupported catalyst determined by total nitrogen analysis, M_{GaN} and $M_{Ga_2O_3}$ denote the molar mass of GaN

(83.73 g mol^{-1}) and Ga_2O_3 (187.44 g mol^{-1}), respectively. $n_N = \frac{N}{M_N}$, with N as the total nitrogen content in g_N g_{cat}^{-1} and M_N as the molecular weight of nitrogen (14.01 g mol^{-1}).

This method, however, could not be applied for the supported catalysts because HCl could not leach out gallium salt from the SBA-15 support. Using fusion flux, the silica structure was completely disintegrated, and gallium was completely extracted, but the nitrogen was lost as ammonia gas.

X-Ray Diffraction (XRD) was used to identify the crystallinity of the catalyst. Analyses were conducted on a Bruker D8 Discovery X-Ray Diffractometer with a two-dimensional VANTEC-500 detector and CuK_α (λ = 1.5406 Å) radiation source. The tube voltage was 40 kV, tube current 20 mA, and scan rate 5° min^{-1}.

Nitrogen adsorption/desorption measurements (–196°C) were conducted using Micromeritics Tristar 3000 BET analyzer to determine total surface area, pore size distribution, and pore volume. Before the analysis, the samples were degassed under vacuum for 12 h at 250 °C. Surface areas of the catalyst were calculated following the BET method.

High-resolution transmission electron microscopy (HRTEM) of fresh and spent catalysts was carried out on FEI Tecnai G2 F20 with 200 kV. Prior to the analysis, a catalyst suspension in ethanol was prepared by sonicating 1–2 mg of the catalyst in 2 mL anhydrous ethanol. Energy-

dispersive X-ray spectroscopy (EDS) was also carried out for detecting the elements present in the catalyst (qualitative).

Scanning Electron Microscopy (SEM) analysis for the unsupported catalyst (Ga_2O_3) was performed using a FEI Inspect F-50 field emission scanning electron microscope. In addition, Energy-Dispersive X-ray Spectroscopy (EDS) experiments were performed for elemental analysis (Ga, N, O, and C).

Temperature programmed oxidation coupled with mass spectrometry (TPO-MS) was carried out for the fresh and spent catalysts to estimate the carbon either deposited during methane activation or catalyst synthesis. Around 50 mg of supported catalyst or 250 mg of unsupported catalyst was placed in a quartz tube (9 mm OD × 7 mm ID × 275 mm long and 15-40 µ frit) and heated in the presence of air (Ultra Zero Air, MEGS Specialty Gases, 22 $mL_N\ min^{-1}$) to 950 °C with a heating rate of 5 °C min^{-1}. The product gas at the reactor outlet was electrically heated to 200 °C, mixed with Ar (MEGS Specialty Gases, 10 $mL_N\ min^{-1}$), and then subsequently analyzed by a mass spectrometer (Pfeiffer Omnistar GSD 301) calibrated for CO_2 (m/z = 44). The gas flow rates were controlled by respective calibrated Vögtlin red-y smart controllers (± 0.3 % accuracy, Switzerland).

In addition, temperature-programmed oxidation with thermogravimetric analysis (TPO-TGA) was carried out for both fresh and spent catalysts (Q500 TA Instrument). 20–25 mg of catalyst was

first purged for 30 min with N_2 at room temperature to remove air from the system and then heated at the rate of 5 °C min^{-1} to 120 °C to remove the moisture. After a holding for 30 min at 120 °C, the sample was then heated to 950 °C at 5 °C min^{-1} in the presence of air and held at 950 °C for 30 min, while the weight change was recorded.

Catalyst synthesis (both unsupported and supported) and the subsequent analyses (BET, XRD, ICP) were repeated for confirming repeatability and reproducibility.

2.3 Catalytic activity measurements

The catalyst performance was measured in a vertical packed bed reactor at 700 °C and 1 bar_{abs}. A quartz tube (9 mm OD × 7 mm ID × 335 mm long) with a 15-40 µ frit at one end was used as the reactor inside a vertical tube furnace (Mellen Company). Around 500 mg of unsupported or 100 mg of supported catalysts were loaded in order to achieve the same bed height of 11 ± 1 mm and the same residence times of 1.3 s (superficial gas velocity at 700 °C) for both catalysts. The bulk densities of the GaN and GaN/SBA15 were 1300 kg m^{-3} and 260 kg m^{-3}, respectively. The inlet gas contained 80 vol% CH_4 (99.999%, Praxair) in Ar (99.999%, MEGS Specialty Gases), which were mass flow controlled using calibrated Vögtlin red-y smart controller (± 0.3% accuracy, Switzerland). The resulting CH_4-based gas hourly space velocities (GHSV) were the same for both GaN and GaN/SBA15 with a value of 567 h^{-1}. The reactor outlet and transfer lines were electrically heated at 200 °C to avoid condensation of the organic components (i.e., C_6H_6, C_7H_8,

$C_{10}H_8$). A quadrupole mass spectrometer (Pfeiffer Omnistar GSD 301) was used for product gas analysis; the instrument was calibrated for methane (CH_4), ethylene (C_2H_4), propylene (C_3H_6), benzene (C_6H_6), toluene (C_7H_8), naphthalene ($C_{10}H_8$), carbon dioxide (CO_2) and hydrogen (H_2) with argon (Ar) as the internal standard (additional details are in the supplementary information). The calibration of the mass spectrometer was verified by a calibrated gas chromatograph (SRI GC 8610) for CH_4, H_2, and C_6H_6 (Fig. S1).

Prior to heating, the catalyst was purged with Ar (25 $mL_N\ min^{-1}$) for 1 h, then heated to 700 °C at a rate of 5 °C min^{-1}, and subsequently, CH_4 was added. The internal reactor temperature (i.e., within the catalyst bed) was measured by a K-type thermocouple (Omega), which was used to control the furnace.

Based on a detailed mass spectrum analysis and calibration factors, the CH_4 conversion, the product molar flow rates (μmol min^{-1} g_{Ga}^{-1}) as a function of time on stream were determined (Fig. 6 and 7). Besides ethylene (C_2H_4), other hydrocarbons such as propylene (C_3H_6), benzene (C_6H_6), toluene (C_7H_8) and naphthalene ($C_{10}H_8$; see Fig. S16) were detected and quantified. The CH_4 conversion was calculated based on the gaseous carbon products (equation 4).

$$x_{CH_4} = \frac{\sum \nu_i \cdot \dot{n}_i}{\dot{n}_{CH_4,in}} \times 100 \quad (4)$$

Where $\dot{n}_i$ denotes the molar flow rate in μmol min^{-1}, while ν_i denotes the number of carbon atoms in the i^{th} species in the product stream (i.e., C_2H_4, C_3H_6, CO_2, C_6H_6, C_7H_8, and $C_{10}H_8$). The

denominator represents the molar flow of methane in the feed (μmol min^{-1}). The conversion closely represents the percentage (%) of carbon (C) converted to hydrocarbons and not coke. Results reported in this work for the methane activation were consistent within 5% of C and H elemental balances.

Reactivity experiments were repeated with the catalyst prepared from the same as well as from different batches. The unsupported catalysts showed good repeatability and reproducibility, as illustrated in Fig. S2A and B. The supported catalysts exhibited a slightly larger deviation for different catalyst batches (Fig. S2C and D) that could be attributed to the incipient wetness impregnation step, which is limited by slower redistribution of Ga inside the pores.

3 Results and discussion

3.1 Nitridation of unsupported catalysts

The nitridation study for unsupported catalysts was divided into two parts, to investigate (1) the effect of nitridation temperature, and (2) the effect of NH_3 exposure time at a fixed temperature (750 °C). In the first part, the temperature was increased under the NH_3 atmosphere, while in the second study, NH_3 was added after the target temperature of 750 °C was reached (under Ar atmosphere). During the nitridation, water is produced ($Ga_2O_3 + 2\ NH_3 \rightleftharpoons 2\ GaN + 3\ H_2O$), which was recorded by mean of mass spectrometry (H_2O, m/z = 18). The first study was a combination of a temperature-programmed reaction with an extended soak time at five different temperatures

to determine the onset and peak temperature for the Ga_2O_3 nitridation and the optimum condition. The results clearly indicate that the nitridation started above 600 °C and that the maximum H_2O formation rate was close to the targeted nitridation temperature for T_{Nit} = 650-800 °C (Fig. 1A). No maximum was observed for 600 °C, indicating a very slow nitridation rate. For nitridation temperatures of 750 and 800 °C, the water signal dropped after 8-10 h to the same level resulting in a very similar Ga_2O_3 conversion, which was confirmed by the total nitrogen analysis (~88 ± 5%, Fig. 1A and B).

For GaN-650 and GaN-700, the water production rate (i.e., Ga_2O_3 conversion rate) was significantly slower, and even after a total NH_3 exposure time of 24 h, the Ga_2O_3 conversions were 46 ± 5% and 70 ± 5%, respectively (Fig. 1B). XRD analyses confirmed the trend as a distinct transition from β-Ga_2O_3 to GaN with increasing nitridation temperature was observed (Fig. 1C). The catalyst nitridated at 600 °C exhibited predominately broad XRD pattern of β-Ga_2O_3 (2θ = 31.7°, 35.2°, 38.4°, and 64.7°; PDF file #00-006-0523 from the International Centre for Diffraction Data). The XRD pattern for the samples treated at 650 °C started to show clear diffraction pattern of GaN (2θ = 32.5°, 36.9°, and 57.9°; PDF file # 04-013–1733) with only minor peaks for β-Ga_2O_3. At nitridation temperatures of 700 °C and higher, the catalyst samples had only diffraction patterns corresponding to GaN, even though the Ga_2O_3 conversion was only between 70-90%.

Based on this result, a nitridation temperature of 750 °C was sufficient as complete bulk conversion might not be necessary for the methane conversion. The nitridation reaction is thermodynamically unfavorable and highly endothermic as indicated by the large positive standard Gibbs free energy and heat of reaction ($\Delta G_{R,298K} = 191.8\ kJ\ mol^{-1}$ and $\Delta H_{R,298K} = 238.2\ kJ\ mol^{-1}$) [23]. However, the significant excess of ammonia, the removal of gaseous products (water), and higher temperatures (750 and 800 °C) resulted in an 88% conversion of Ga_2O_3 to GaN (Fig. 1B). For lower temperatures (with the same gas flow rates), the Ga_2O_3 conversion was significantly smaller (by around 50%), indicating that more time and/or higher temperature was needed. Moreover, not all Ga was accessible for NH_3 due to collapsing of the pores.

In the second study, the Ga_2O_3 samples were exposed to NH_3 for 3 h, 6 h, or 9 h after the desired nitridation temperature of 750 °C was achieved. The results are illustrated in Fig. 1D, E, and F. The H_2O signal increased instantaneously at the onset of the nitridation and then declined rather fast with time. The longer the nitridation time, the smaller the H_2O signal, and the higher the Ga_2O_3 conversion (i.e., 64% at 3 h vs. 85% at 9 h, see Fig. 1D and E). XRD analyses of these three samples showed only diffraction patterns corresponding to GaN (Fig. 1F). Even with a Ga_2O_3 conversion of only 64% at 3 h NH_3 exposure time, the peaks corresponding to oxide (β-Ga_2O_3) were not visible. It has been suggested that the conversion of β-Ga_2O_3 to GaN proceed either

through the formation of amorphous gallium oxynitride (GaO_xN_y) intermediates or via Ga_2O [24]. The latter Ga_2O as gas phase intermediate is assumed at temperatures higher than 900 °C.

Nitrogen adsorption/desorption analysis of all unsupported Ga_2O_3 and GaN catalysts exhibited type-IV isotherms with H3 and H4 type hysteresis loops with bimodal pore size distribution (Fig. S3). The disordered structure was also observed for Ga_2O_3 synthesized by the EISA method [25]. Table 1 summarizes BET surface areas and pore volumes, as well as two pore sizes with the highest contributions. The Ga_2O_3 had a surface area of 19 $m^2\ g^{-1}$ and a pore volume of 0.08 $cm^3\ g^{-1}$ with a bimodal pore size distribution of 7.5 and 31.5 nm. More than 85% of the surface area corresponded to meso- and macropores, while the rest were micropores.

Upon nitridation at 650 °C, the surface area decreased by ~20% down to 15 $m^2\ g^{-1}$ with a pore volume of 0.075 $cm^3\ g^{-1}$. This was probably due to the change from the monoclinic crystal structure of β-Ga_2O_3 to the wurtzite structure of GaN. A further decrease of the surface area to 11 $m^2\ g^{-1}$ at $T_{Nitridation}$ of 800 °C could be attributed to sintering and/or pore structure collapse due to the crystallization of GaN at temperatures above the calcination temperatures [26]. Commercial GaN powder had a slightly smaller surface area with S_{BET} = 8 $m^2\ g^{-1}$ than catalyst prepared in this work [20].

TEM and EDS analysis for Ga_2O_3 and GaN-650 are illustrated in Fig. 2. Both gallium catalysts are an agglomeration of nanoparticles with polycrystalline structure, as depicted with the darkfield

in the top-left insets of Fig. 2A and B. The nanoparticle size ranges from 20 to 200 nm (Fig. S4). Polycrystalline Ga_2O_3 has several characteristic d-spacings representing the monoclinic structure (cell dimensions of $a = 12.23 \pm 0.02$, $b = 3.04 \pm 0.01$, $c = 5.80 \pm 0.01$ Å and $\beta = 103.7 \pm 0.3°$)[27]. Fig. 2 and S5 visualizes d-spacings of 3.0 ± 0.1 and 6.0 ± 0.1 Å corresponding to the [001] plane [28] as well as 9.9 Å associated with the [010] plane [29].

The synthesized GaN-650 catalyst had a Ga_2O_3 conversion after the nitridation of around 46 %; thus, as expected, both GaN and Ga_2O_3 phases were visible in the TEM, with a possible core-shell structure of Ga_2O_3 in the center (Fig. 2B and S6). GaN has a regular wurtzite structure with both *m*- and *c*-planes. The *m*-plane is non-polar and made of alternating Ga and N ions, while the *c*-plane is polar containing either Ga or N ions. The lattice parameters of the *m*-plane with 5.2 Å, as well as the hexagonal structure of the *c*-plane with $\sqrt{3}a = 5.5$ Å could be observed, as illustrated in Fig. 2B and Fig. S7, respectively. For the amorphous Ga_2O_3 part, a *d*-spacing of 9.9 Å was measured. An amorphous gallium oxynitride (GaO_xN_y) might exist at the boundary between GaN and Ga_2O_3.

Fig. 2C depicts the EDS for fresh Ga_2O_3, and fresh and spent GaN-650 catalysts. As expected, the pure Ga_2O_3 sample had no peaks corresponding to nitrogen and much higher oxygen counts than both of the GaN-650 samples (fresh and spent) that contain GaN as well as Ga_2O_3 phases. The spent GaN catalyst had a higher carbon peak and, consequently, smaller peaks associated with

nitrogen and oxygen, confirming the presence of carbonaceous material deposition. Some contributions to the carbon signal and all the copper count were from the sample grid. The EDS data shown were normalized based on the gallium count and semi-quantitative in nature.

3.2 Nitridation of supported catalysts

Supported gallium oxide (Ga_2O_3/SBA15) samples showed a slightly higher H_2O signal upon nitridation when compared with SBA-15 without gallium oxide (GaN/SBA15 vs. N-SBA15 in Fig. 3A). But no maximum was observed, which was probably due to the lower Ga_2O_3 content (around 35 mg compared to 1000 mg for the unsupported Ga_2O_3 loaded for nitridation). As mentioned above, the degree of nitridation (i.e., Ga_2O_3 conversion) by total nitrogen analyses of the product (GaN/SBA15) could not be determined.

The nitridated gallium-containing supported catalysts showed the presence of crystalline GaN but did not exhibit any peak corresponding to β-Ga_2O_3 (Fig. 3B). Even for the Ga_2O_3/SBA15 samples, no diffraction pattern for β-Ga_2O_3 was observed, indicating very small non-crystalline particles. The XRD peak around $2\theta = 44°$ (Fig. 3B) corresponds to the aluminum sample holder of XRD.

Although the total N could not be performed for the supported catalysts, the peaks corresponding to the nitrides are sharper at all nitridation temperatures compared to the unsupported catalysts (GaN-600 and 650). Since the total Ga content in the supported catalyst was much lower, it can be assumed that the conversion of Ga_2O_3 to GaN was near completion for all samples.

The prepared support SBA-15 had a total BET surface area of 912 m^2 g^{-1} (~20% micro and ~80% mesopores), which decreased to 420 m^2 g^{-1} (~15% micropores) when nitridated at 800 °C (N-SBA15-800). This might be due to partial pore collapse at higher temperatures, as shown by the reduced pore volume (i.e., from 0.89 to 0.61 cm^3 g^{-1}). Adding Ga to the support (including impregnation and calcination at 550 °C) also reduced the total surface area to 426 m^2 g^{-1} and pore volume to 0.53 cm^3 g^{-1} but did not change the average pore size (Table 2). Moreover, the data show that the share of the micropore surface area decreased from 20% to 13%.

The surface areas of Ga_2O_3/SBA15 was still 20 times larger than for the unsupported catalyst samples with a value of 19 m^2 g^{-1} (see Ga_2O_3 in Table 1). Thus, it was easier for NH_3 to access Ga_2O_3 resulting in most likely in a higher conversion during the nitridation, especially at lower temperatures.

Upon nitridation up to 700 °C, the surface area did not change much, but the average pore size decreased from 7.9 to 6.4 nm when compared to the Ga_2O_3/SBA15 sample. An increase in the nitridation temperature above 750 °C (i.e., GaN/SBA15-750 and 800) resulted in the reduction of the total surface area down to 320 m^2 g^{-1}. The share of micropores decreased even further to 8%. At higher nitridation temperatures, the surface area reduction was most likely due to a combination of sintering of GaN particles and pore structure collapsed [26].

Compared to the unsupported catalyst (GaN), the supported catalysts (GaN/SBA15) had a unimodal pore size distribution at around 6.4 nm (Table 2, Fig. S9).

Based on ICP analyses, Ga-loadings of 13 ± 1 wt% in Ga_2O_3/SBA15 (target 16 wt% Ga) and 11 ± 1 wt% in GaN/SBA15 were determined. The loss of around 3 wt% from the target loading could be attributed to the loss of gallium nitrate solution during catalyst synthesis.

HRTEM was carried out for Ga_2O_3/SBA15, GaN/SBA15-650, and GaN/SBA15-800 catalysts, both fresh and spent (Fig. 4 and Fig. S10). For the fresh Ga_2O_3/SBA15, no gallium nanoparticles were observed, while the ordered hexagonal pore structure of the SBA-15 was clearly visible with a size of around 8 nm (same as determined by BET measurement see Table 2). In EDS, however, the presence of Ga was confirmed (Fig. 4D). This suggests that the Ga_2O_3 nanoparticles were highly amorphous as supported by XRD results for the Ga_2O_3/SBA15 (Fig. 3B). GaN, on the other hand, was clearly distinguishable from the SBA-15 in the TEM, as depicted in Fig. 4B and C for GaN/SBA15-650 and 800, respectively. Moreover, Fig. 4B and C show clearly that the GaN nanoparticles (3-5 nm, Fig. 4 B and C) were inside the 6-8 nm pores of the SBA-15 support. XRD measurement confirmed that GaN had a crystalline structure (see Fig. 3B).

Although the spent GaN/SBA15-800 did not show much change in morphology, several agglomerations of particles inside the hexagonal array of pores for the spent GaN/SBA15-650 were observed with the TEM (see Fig. S10B). These agglomerations were most likely carbon deposition due to coking during the methane conversion. EDS analysis (Si normalized) confirmed that the spent GaN/SBA15-650 catalyst had a much higher carbon count than the fresh catalyst

(Fig. 4D). Consequently, the peak corresponding to Ga was significantly smaller in the spent than in the fresh catalyst.

3.3 Activity measurements over unsupported catalysts

Mass spectrum analyses revealed that the Ga_2O_3 sample produced amount of H_2O (m/z =18) and CO_2 (m/z =44) in the first hour during the methane activation (Fig. 5A to D), while the nitridated catalysts did not exhibit any formation of H_2O and CO_2 (Fig. 5E to H and Fig. S11 for GaN-750). The GaN-600 sample showed an insignificant amount of H_2O and CO_2, (see Fig. S12), even though this sample contained ~65% of Ga_2O_3. This may indicate that during the nitridation, mostly the outer surface of the low porosity Ga_2O_3 was converted to GaN, while the bulk remained Ga_2O_3 (core-shell structure).

This also explains the different behavior of the H_2 formation (m/z = 2) for the Ga_2O_3 (max. H_2 at 2 h) and GaN (max. H_2 at < 1 h) samples. During the induction period, CH_4 produced H_2O, CO, and CO_2 on Ga_2O_3, creating an oxygen vacancy in the crystal lattice, also predicted by our DFT work [21]. SEM-EDS analysis of fresh and used Ga_2O_3 catalysts (Fig. S13 and S14) showed only a marginal loss of oxygen within the error of estimation. Also, the XRD for fresh and spent Ga_2O_3 were practically indistinguishable, indicating no change in the crystal structure (Fig. S15).

Since CO and C_2H_4 have the same nominal mass (m/z =28), it was impossible to distinguish between them via mass spectrometry. CO and CO_2 might have been formed via gallium-methoxy

species ($Ga–O–CH_3$) that were experimentally observed via ^{13}C NMR over Ga-modified zeolites [10]. However, the number of methoxy groups are assumed to be much smaller than the gallium-methyl species. The reaction pathway towards CO and CO_2 has been reported by Chaudhari et al.[21]. It has been shown that gallium oxide is active towards the reverse water-gas shift reaction during the alkane dehydrogenation in the presence of CO_2 [30]. Assuming the reverse water-gas shift reaction at equilibrium, the maximum CO formation and hence the minimum C_2H_4 formation rates could be determined. Since negligible amounts of H_2O and CO_2 were observed for the nitridated samples, the mass-to-charge ratio m/z = 28 was associates with C_2H_4 only (Fig. 5E to F).

All unsupported catalyst samples exhibited similar behavior in terms of CH_4 conversion as well as product formation rate except ethylene. The ethylene rates were higher for the nitridated catalysts when compared with the oxide precursor (Ga_2O_3), but the rates were similar within the nitridated samples from 600-800 °C. At the onset of the reaction, CH_4 conversion values of 4% were determined, which rapidly decreased to less than 1% after 3 h on stream. The steady-state rate attained was up to 0.1 $mmol_{CH4}\ h^{-1}\ g_{Ga}^{-1}$.

C_2H_4 had the highest hydrocarbon-based formation rate at the beginning of the reaction with up to 5 $\mu mol\ min^{-1}\ g_{Ga}^{-1}$ that was 3 to 4 orders of magnitude larger than for the other hydrocarbons. Benzene formation rates were about 100 times smaller, while the rates for propylene, toluene, and

naphthalene (Fig. S16) were more than 1000 times lower. The maximum hydrocarbon and H_2 formation rates for the nitridated catalysts occurred within the first hour, while the non-nitridated catalyst (Ga_2O_3) had longer induction time with an observed the maxima between 1 and 2 h (Fig. 6 and 7).

Independent of the nitridation temperature and time, all unsupported catalysts deactivated faster within 3-5 h due to coking (Fig. 6 and 7), which was evident from the color change from yellow (fresh GaN) or white (fresh Ga_2O_3) to black (spent, Fig. S17) as well as the temperature-programmed oxidation results (see below). The degree of nitridation influenced slightly more the formation rates of aromatic compounds (C_6H_6 and C_7H_8) than of olefins (C_2H_4 and C_3H_6). The Ga_2O_3 catalyst had the lowest C_6H_6 and C_7H_8 formation rates, followed by the catalyst nitridated 600 °C (GaN-600). GaN-700 and GaN-750 exhibited the highest C_6H_6 and C_7H_8 formation rates.

If C_2H_4 would be the only hydrocarbon product, the ratio of the observed H_2 to C_2H_4 formation rates should be 2, corresponding to the stoichiometric factor shown in equation 5.

$$2\ CH_4 \rightarrow C_2H_4 + 2H_2 \qquad (5)$$

For the unsupported catalysts, the ratio of hydrogen and ethylene formation rate changed with time, as illustrated in Fig. S18A and B. At the onset, the ratio was close to two, while it increased to a maximum of 7-12 depending on the catalyst after 1 to 2 h on stream. Afterward, the ratio attained a value of 3 at the end of the run. The ratio was higher than 2; thus, more H_2 was formed,

indicating that a considerable amount of hydrocarbons were adsorbed on the catalyst surface as CH_x* or C_yH_z* species with a yet unknown stoichiometry. Since the C_2H_4 formation rate was a factor of 100 to 1000 larger than the other gaseous hydrocarbons, they would not influence the observed H_2/C_2H_4 ratio significantly. No methane activation was observed when the reaction was carried out in an empty quartz reactor (blank experiments); therefore, homogeneous gas phase reactions were negligible at 700 °C.

A single CO_2 peak at 467 ± 5 °C for the spent Ga_2O_3 was observed during temperature-programmed oxidation (TPO-MS), which shifted slightly to higher temperatures 480 ± 6 °C for the GaN catalysts as illustrated in Fig. 8. A H_2O peak (m/z = 18) was observed at the same temperature (Fig. S19A). Based on this temperature range, it can be assumed that the carbonaceous material was rather amorphous instead of graphitic carbon, which requires higher oxidation temperatures [31]. In addition, the single CO_2 peak indicates a single carbon surface species that behaved similarly on the GaN and Ga_2O_3 samples under an oxidizing atmosphere. TPO-TGA measurements of the spent samples confirmed the results, as depicted in Fig. S20A and B. Interestingly, at temperatures above 550 °C the weight of the used GaN samples increased due to the oxidation to Ga_2O_3, which was also observed in our previous study [20].

The quantitative analysis of the spent catalyst after 5 h yielded a relative carbon amount of 22 mg g_{cat}^{-1} for Ga_2O_3 and 10-16 mg g_{cat}^{-1} for GaN catalysts (Table S1).

Based on the TPO analysis and product gas composition data, the overall selectivities for the adsorbed carbon as well as specific selectivities and total C_2H_4 yield were determined and summarized in Table 3. It is evident that the adsorbed carbon/coke, yet with an unknown C_xH_y stoichiometry, was the primary product, whereas the total hydrocarbon selectivity was between 30-50 mol%. The hydrocarbons itself were predominately C_2H_4 with selectivity values of up to 49 mol% for GaN-750-03 and 27 to 34 mol% for Ga_2O_3. For the latter, a range was calculated indicating the minimum and maximum value for C_2H_4 selectivity depending on the influence of the reverse water-gas shift reaction and thus CO formation. C_6H_6 and C_3H_8 selectivities ranged from 0.5 to 0.9 mol% and 0.1 to 0.3 mol%, respectively.

To put these results in context, the equilibrium composition was calculated with the assumption of CH_4 as the only reactant and H_2, C_2H_4, and C_3H_6 as the only products. Aromatic compounds benzene, toluene, and naphthalene being less than 100 times than C_2H_4 had not been considered in the calculations. Thermodynamically, the maximum CH_4 conversions and C_2H_4 yields (without coke) are 4.1% and 3.5% at 700 °C, 9.1%, and 8.1% at 800 °C and 17.0% and 15.5% at 900 °C, respectively (see Fig. S21). Carbon deposition was excluded from the conversion calculations (Fig, 6) as the molar rates of surface intermediates were not measured as a function of time. Methane conversion based on carbon incorporated in the products (excluding coke) can be compared with the equilibrium calculations (Fig. S21). The equilibrium calculations did not

include coke. The steady-state conversion (Fig. 6) was less than 10% of the equilibrium conversion (Fig. S21).

3.4 Activity measurements over supported catalysts

Unlike unsupported Ga_2O_3 catalyst, the supported Ga_2O_3/SBA15 sample produced H_2O and CO_2 in the first hour on stream, while the nitridated catalysts did not produce a significant amount of CO_2 and H_2O (Fig. 9 and Fig. S22).

The main hydrocarbon product of the supported catalysts was again ethylene (C_2H_4), as depicted in Fig. 10. Supported GaN catalysts were very selective for the direct non-oxidative methane dehydrogenation and subsequent coupling to ethylene. Propylene and benzene were approximately 100 and 1000 times smaller, respectively. Unlike the unsupported catalyst, the initial CH_4 conversion was less than 1%, and then decreased to less than 0.5%, and remained steady (Fig. 10A). Similar CH_4 conversions (< 0.3%) were reported by Dumesic's group over PtSn-zeolite catalysts [32]. The supported GaN/SBA15 deactivates slower than the unsupported GaN, at the initial reaction stage. The steady-state rate attained was between 1.5-3.0 $mmol_{CH4}\ h^{-1}\ g_{Ga}^{-1}$ (equivalent to 0.2-0.4 $mmol_{CH4}\ h^{-1}\ g_{cat}^{-1}$), which was at least 10 times the unsupported catalysts. The rate is comparable to the rate reported by Sheng et al. [14] with 0.3 $mmol_{CH4}\ h^{-1}\ g_{Cat}^{-1}$.

The supported catalysts were more stable than the unsupported. Moreover, the C_2H_4 and C_3H_6 formation rates per gram of Ga were about 10 and 100 times higher for the supported catalyst (Fig. 6 vs. 10), respectively. The supported catalyst had more than 20 times higher porosity than the unsupported samples (see Tables 1 and 2). Moreover, GaN within the SBA-15 structure was very well dispersed with a crystallite size of 3-5 nm (from Fig. 4 B and C), whereas the unsupported GaN consists of an agglomeration of nanoparticles with 20–200 nm (Fig. S4). The latter had a much lower Ga dispersion and, therefore, a much lower rate per mass of gallium. It seems that methane coupling to ethylene over GaN is structure sensitive.

After approximately 1 h, the CH_4 conversions were in steady-state and corresponded to the hydrocarbon formation rates (specifically C_2H_4). This indicates that the active catalyst surface might have been covered with CH_4 during the initial phase, which has been confirmed by TGA experiments, as reported in our work [33]. This was also suggested by Xiao and Varma [12].

The Ga_2O_3/SBA15 and GaN/SBA15-650 exhibited higher CH_4 conversions compared to the samples nitridated at 700 to 800 °C (GaN/SBA15-700 to GaN/SBA15-800, Fig. 10A). However, the H_2 formation rate differs significantly. For Ga_2O_3/SBA15, the H_2 production rate increased from 43 to 68 µmol min^{-1} g_{Ga}^{-1} within 7 h of reaction time. At the same time, the H_2O formation decreased (Fig. S22). Since no water was produced over the nitridated samples, the H_2 formation rates were constant with GaN/SBA15-650 achieving the fastest rate of ~110 µmol min^{-1} g_{Ga}^{-1} and

GaN/SBA15-700 the slowest rate of ~40 µmol min^{-1} g_{Ga}^{-1}. The C_2H_4 production rate exhibited a similar trend as observed for H_2, highest steady-state rate of 22 µmol min^{-1} g_{Ga}^{-1} for GaN/SBA15-650, and lowest of 12 µmol min^{-1} g_{Ga}^{-1} for GaN/SBA15-700. Minor components such as C_3H_6, C_6H_6, and C_7H_8 were 100–1000 times lower than C_2H_4, similar to their unsupported counterparts.

The ratio of the H_2 and C_2H_4 formation rates over the supported samples were close to three and did not change significantly with time on stream (Fig. S18C). This value was much smaller than for the unsupported gallium catalysts indicating that over supported gallium catalysts less adsorbed carbon surface species (i.e., CH_x*) were formed. Since the behavior for the unsupported and supported GaN catalysts were different (i.e., supported catalyst was more stable), it is assumed that the adsorbed carbonaceous species was not catalytically active.

Temperature programmed oxidation - mass spectrometry (TPO-MS) analyses of the spent catalysts showed a major CO_2 peak at 600 ± 10 °C, as illustrated in Fig. 11. This was around 120 °C higher than for the unsupported catalysts (Fig. 11 vs. 8). The same behavior was observed by means of thermogravimetric experiments (TPO-TGA, Fig. S20) as well as by determining the produced water via mass spectrometry (Fig. S19). For the latter, the H_2O signal corresponded perfectly to the CO_2 peaks. The reason for the higher temperature might be the confinement effect due to the small pore size of the supported catalysts (6 nm). A similar effect has been reported for Mo-containing zeolites [34]. A different adsorbed carbon surface species with a stronger carbon-

catalyst bond than for the unsupported catalysts might be possible as well. The presence of polyaromatic compounds inside SBA-15 pores cannot be ruled out, as observed in [35]. However, in the present case, the rate of ethylene formation was by a factor of 1000 higher than the rate for benzene and toluene formation (Fig. 10). Thus, it is more likely that the carbon surface species were CH_x instead of polyaromatic. The small CO_2 peak between 300 and 400 °C was observed in all samples, including the fresh catalysts. It most likely was a remnant of the copolymer.

The weight changes determined with TPO-TGA agreed with TPO-MS analyses, as summarized in Table S2 and S3. For example, GaN/SBA15-700 had 5.8 $mg_C\ g_{cat}^{-1}$ and 6.5 $mg_{CH}\ g_{cat}^{-1}$ based on TPO-MS and TPO-TGA, respectively. Ga_2O_3/SBA15 had 17.9 $mg_C\ g_{cat}^{-1}$ and 21.5 $mg_{CH}\ g_{cat}^{-1}$ based on TPO-MS and TPO-TGA, respectively. The results for the TPO-MS analyses were slightly lower, as it was based on CO_2 (i.e., carbon) only, whereas TPO-TGA was based on the weight loss (i.e., carbon and hydrogen included). Gerecke et al. reported much higher carbon depositions of 43 to 120 $mg_C\ g_{cat}^{-1}$ for the non-oxidative methane coupling to ethylene over PtSn-zeolite catalysts [32].

Based on the TPO results, the overall carbon-based selectivities (i.e., C_2H_4, C_3H_8, C_6H_6, C_7H_8, $C_{10}H_8$, and adsorbed carbon C_{ads}) were determined and summarized in Table 4 together with the overall CH_4 conversion and C_2H_4 yield.

The nitridated support without any gallium (N-SBA15-800) did not exhibit any methane activation, which was also evident from the color of the used catalyst, which was white same as the fresh catalyst (not shown). All supported catalysts achieved a higher C_2H_4 overall selectivity than the unsupported catalysts (43-70% vs. 30-49%). The GaN/SBA15-700 and 750 catalysts had the highest C_2H_4 selectivity with 70%, but the lowest yields due to the lower CH_4 conversion. However, the Ga_2O_3/SBA15 and GaN/SBA15-650 catalysts had a considerably higher adsorbed carbon (coke) content. In addition, the Ga_2O_3/SBA15 produced a significant amount of carbon oxides and water.

Less than 0.5 mol% of the total methane feed added was converted to adsorbed carbon (e.g., CH* or CH_2^*) within 7 h time on stream. After 7 h on stream, the adsorbed carbon to gallium molar ratio was about $C_{ads}/Ga = 1 \pm 0.05$ for GaN/SBA15-650 and Ga_2O_3/SBA15. With increasing nitridation temperature the ratio decreased to $C_{ads}/Ga = 0.25 \pm 0.05$ for the GaN/SBA15-700, -750 and -800 samples. For the nitridated samples, this might indicate that the adsorbed carbon species (CH* or CH_2*) are site-selective [36]. Based on this, a Ga dispersion of approximately 25% can be estimated for the supported catalyst that has GaN cluster sizes of 3-5 nm (from Fig. 4 B and C).

The turnover frequency (TOF) could not be calculated as the active surface area (number of actives sites) could not be determined via standard chemisorption using CH_4 and CH_4-TPD techniques

(not shown). CH_4 did not chemisorb at low temperatures (25-45 °C). Our DFT results [21] indicated that the first step of CH_4 activation involved weak adsorption on the *m*-plane of the GaN, with carbon weakly bonded to Ga, forming a Ga−C bond following the alkyl mechanism [18,21]. A similar result was obtained for Ga_2O_3, with carbon bonded to Ga while one H attracted to O (alkyl mechanism) [21]. CH_4 can also adsorb via the carbenium mechanism [10] to form a methoxy group, Ga−O−CH_3; however, based on the DFT calculation, the carbenium mechanism was not favored. This was also in agreement with in-situ ^{13}C solid-state NMR spectroscopy experiments conducted over Ga/H-BEA by Luzgin et al. [10]. They showed that gallium-methyl species (Ga−CH_3) was the major surface intermediate, and gallium-methoxy was only a minor surface species. Our DFT results implied that CH_4 did not adsorb on GaN and Ga_2O_3 as a molecule but through dissociative adsorption. This confirms that CH_4-TPD and CH_4 chemisorption techniques failed to determine the number of active sites at low temperatures. Based on the experimental results [33] as well as our reported DFT simulations [21], it is hypothesized that CH_4 undergoes fast dissociative adsorption on all the active sites (R1 to R3, Fig. 12) for GaN and Ga_2O_3. The active CH_3* surface intermediate is further dehydrogenated to CH_2* with the release of H_2 (R4 and R5 in Fig. 12), which are the rate-determining steps, and then dimerized to C_2H_4. The CH_2 surface intermediate can be further dehydrogenated to CH* and C* (R7, Fig. 12), which might lead to undesired coke. For the Ga_2O_3 catalysts, H_2O is formed via R3′, leaving a vacant site (Fig.

12B). The carbon oxides are produced from the interaction of adsorbed CH_2* (on Ga) with neighboring top layer oxygen atoms [21].

To summarize, catalyst nitridation was needed for two reasons: (1) over gallium oxide H_2O and CO_x were formed in addition to C_2H_4, leading to lower C_2H_4 selectivity ($S_{C_2H_4}$, Fig. 13), and (2) nitridation reduced the carbon deposition (C_{ads} Fig. 13). Hence, nitridation improved the atom conversion efficiency for CH_4 carbon, and the efficiency was higher for the supported catalyst. In the case of unsupported catalysts, the nitridation temperature affects directly the nitrogen content (i.e., Ga_2O_3 conversion); however, the degree of nitridation did not influence the methane activity in terms of $S_{C_2H_4}$ and C_{ads} as a complete bulk nitridation was not needed (Fig. 13B). Surface nitridation was sufficient for improving $S_{C_2H_4}$ and reducing C_{ads}. A similar behavior was observed for the supported catalyst (except GaN/SBA15-650); in detail, with higher nitridation temperature ($\geq$ 700 °C) the total surface area decreased, which did not influence the activity in terms of $S_{C_2H_4}$ and C_{ads} (Fig. 13A). There is an additional factor of support basicity in GaN/SBA15 catalysts. Huo et al. [37] have shown that nitridated N-SBA-16 support was more stable and had lower carbon deposition that non-nitridated SBA-16 for Ni/SBA-16 catalysts for methane dry reforming. Depending upon the nitridation temperature, the O atoms in SBA-16 and SBA-15 (silanol OH) are replaced by N (NH_2) [37,38]. The increased basicity in N-SBA-16 resulted in stronger metal-support interaction [37]. As reported by Chino et al. [38], in their work on SBA-15 nitridation, the nitrogen uptake by SBA-15 was negligible below 700 °C. The nitrogen content increased from 2

wt% to 16 wt% from 700 °C to 1000 °C [38]. This explains why our GaN/SBA15-650 had the highest C_{ads} among all the supported nitride catalysts, as the SBA-15 support was not sufficiently nitridated. From Fig. 13, it can be concluded that the optimum nitridation temperatures were 700 °C and 750 °C for the supported and the unsupported catalysts, respectively.

4 Conclusions

For the first time, this work reported the synthesis and characterization of supported GaN/SBA15 catalysts for methane activation to ethylene. Additionally, unsupported GaN catalysts were also synthesized, characterized, and tested for methane activation. The effect of synthesis parameters and catalyst type were investigated on ethylene selectivity and carbon deposition on the catalysts. We addressed the issue of carbon deposition by using a less acidic support. The catalysts produced more ethylene than aromatics and less coke when compared to precious metal and metal oxide catalysts. The unsupported and SBA-15 supported gallium nitride catalysts were synthesized via a simple one-pot procedure and incipient impregnation, respectively, followed by calcination and subsequent nitridation. The influence of the nitridation condition on the catalyst structure and further on the direct non-oxidative methane activation was investigated. With higher nitridation temperature, the Ga_2O_3 conversion to GaN of the unsupported samples increased from 35 to 88%, while the surface area decreased significantly from 19 to 11 $m^2\ g^{-1}$. For the supported catalyst, the Ga_2O_3 conversion to GaN could not be determined; however, since the gallium particles inside

SBA-15 pores were around 3-5 nm (from Fig. 4 B and C), high conversions can be assumed. The total surface area of the supported gallium samples was much larger, which decreased from 420 to 320 m^2 g^{-1} with increasing nitridation temperature.

The unsupported GaN catalysts deactivated rather fast within 3 h, whereas the supported GaN/SBA catalysts were stable and exhibited a steady H_2 and hydrocarbons formation rate for 7 h. The main hydrocarbon product was C_2H_4, with selectivities of up 71 mol% for the supported and 50 mol% for the unsupported samples. The balance was predominantly adsorbed surface carbon and coke. The supported catalysts had 10 times higher C_2H_4 and H_2 formation rate per gram of Ga than the ./.unsupported catalysts. Ga_2O_3 and Ga_2O_3/SBA15 samples had a smaller C_2H_4 selectivity as they produced a significant amount of H_2O and CO_2 through the reaction of the lattice oxygen with CH_4. This was not observed for the nitridated catalysts, even for the GaN-650 sample that contained ~65 % Ga_2O_3.

Higher surface area, well-dispersed GaN in the supported catalysts increased the accessibility of CH_4 to the active sites (GaN). The accessibility to GaN was much lower in practically non-porous unsupported catalysts (even with higher Ga content). In conclusion, based on $S_{C_2H_4}$ and C_{ads}, the catalyst of interest for methane activation and coupling to ethylene is the supported catalyst GaN/SBA15-700.

Supporting information

Comparison between GC and MS results for CH_4, H_2, and C_2H_4 (Fig. S1). Reproducibility results (Fig. S2). Nitrogen adsorption/desorption analysis (Fig. S3 and S9). TEM images (Fig. S4 to S8 and S10). Mass spectra analysis for unsupported catalyst (Fig. S11 and S12). SEM-EDS for fresh Ga_2O_3 (Fig. S13) and spent Ga_2O_3 (Fig. S14). XRD for fresh Ga_2O_3 and spent Ga_2O_3 (Fig. S15). Naphthalene formation rate over unsupported gallium catalyst (Fig. S16). Pictures of fresh and used catalysts (Fig. S17). Ratio of H_2 and C_2H_4 formation rates (Fig. S18). Water evolution during TPO-MS (Fig. S19). TPO-TGA results for spent and fresh catalysts (Fig. S20). Equilibrium conversion of CH_4 and yields of C_2H_4 and C_2H_8 as a function of temperature (Fig. S21). CO_2 and H_2O formation rate of Ga_2O_3/SBA15 and GaN/SBA15-650 (Fig. S22). XRD for spent catalysts (Fig. S23). Adsorbed carbon on spent catalyst (Table S1–3).

Author Contribution Statement

Kanchan Dutta: Conceptualization, Methodology, Validation, Formal Analysis, Investigation, Writing – Original Draft, Writing – Review & Editing, Visualization

Vishnu Chaudhari: Methodology (DFT), Formal Analysis, Investigation, Writing – Original Draft, Writing – Review & Editing, Visualization

Chao-Jun Li: Conceptualization, Investigation, Writing – Review & Editing, Funding Acquisition

Jan Kopyscinski: Conceptualization, Methodology, Validation, Formal Analysis, Resources, Writing – Review & Editing, Visualization, Supervision, Project Administration, Funding Acquisition

Acknowledgments

The authors thank Aleksandra Djuric for conducting the N_2 adsorption/desorption and Ranjan Roy and Andrew Golsztajn for the ICP-OES measurements and helping authors for developing the total nitrogen analysis method. The authors also thank Daniel Pacheco Gutierrez and Obinna Kingsley Uwa for their help with the catalyst synthesis. The authors also thank Mohsen Shahryari for his help with proofreading. J. Kopyscinski acknowledges the financial support from Fonds de recherche du Québec – Nature et technologies (FRQNT, Team Grant PR–253397) and via the Centre in Green Chemistry and Catalysis (FRQNT–2020-RS4–265155-CCVC) as well as from Imperial Oil University Research Award and Natural Sciences and Engineering Research Council of Canada (NSERC CRDPJ 534026). CJ. Li thanks NSERC, Canada Research Chair, and the Fessenden Professorship of McGill University for support of this research.

References

[1] K. Patel, IBISWorld Industry Report 32511 Petrochemical Manufacturing in the US, 2019.

[2] N. Leach, IBIS World Industry Report 32511CA Petrochemical Manufacturing in Canada, 2018.

[3] C. Karakaya, R.J. Kee, Prog. Energy Combust. Sci. 55 (2016) 60–97.

[4] S. Ma, X. Guo, L. Zhao, S. Scott, X. Bao, J. Energy Chem. 22 (2013) 1–20.

[5] P. Tang, Q. Zhu, Z. Wu, D. Ma, Energy Environ. Sci. 7 (2014) 2580.

[6] J.J. Spivey, G. Hutchings, Chem. Soc. Rev. 43 (2014) 792–803.

[7] S. Ma, X. Guo, L. Zhao, S. Scott, X. Bao, J. Energy Chem. 22 (2013) 1–20.

[8] D. Gerceker, A. Hussain Motagamwala, K.R. Rivera-Dones, J.B. Miller, G.W. Huber, M. Mavrikakis, J.A. Dumesic, ACS Catal. 7 (2017) 2088–2100.

[9] E. Mansoor, M. Head-Gordon, A.T. Bell, ACS Catal. 8 (2018) 6146–6162.

[10] M. V. Luzgin, A.A. Gabrienko, V.A. Rogov, A. V. Toktarev, V.N. Parmon, A.G. Stepanov, J. Phys. Chem. C 114 (2010) 21555–21561.

[11] D. Gerceker, A.H. Motagamwala, K.R. Rivera-Dones, J.B. Miller, G.W. Huber, M. Mavrikakis, J.A. Dumesic, ACS Catal. 7 (2017) 2088–2100.

[12] Y. Xiao, A. Varma, ACS Catal. 8 (2018) 2735–2740.

[13] D. Bajec, A. Kostyniuk, A. Pohar, B. Likozar, Int. J. Energy Res. 43 (2019) 6852–6868.

[14] H. Sheng, E.P. Schreiner, W. Zheng, R.F. Lobo, ChemPhysChem 19 (2018) 504–511.

[15] X. Guo, G. Fang, G. Li, H. Ma, H. Fan, L. Yu, C. Ma, X. Wu, D. Deng, M. Wei, D. Tan, R. Si, S. Zhang, J. Li, L. Sun, Z. Tang, X. Pan, X. Bao, Science. 344 (2014) 616–619.

[16] J.S.J. Hargreaves, Coord. Chem. Rev. 257 (2013) 2015–2031.

[17] L. Li, S. Fan, X. Mu, Z. Mi, C.-J. Li, J. Am. Chem. Soc. 136 (2014) 7793–7796.

[18] L. Li, X. Mu, W. Liu, X. Kong, S. Fan, Z. Mi, C.J. Li, Angew. Chemie - Int. Ed. 53 (2014) 14106–14109.

[19] C.-J. Li, Z. Mi, L. Li, Process for Producing Aromatic Compounds Using Light Alkanes, PCT/CA2014/050864, 2015.

[20] K. Dutta, L. Li, P. Gupta, D.P. Gutierrez, C.-J. Li, J. Kopyscinski, Catal. Commun. 106 (2018) 16–19.

[21] V. Chaudhari, K. Dutta, C.-J. Li, J. Kopyscinski, Mol. Catal. In-print (2019).

[22] D. Zhao, J. Feng, Q. Huo, N. Melosh, G.H. Fredrickson, B.F. Chmelka, G.D. Stucky, Science. 279 (1998) 548–552.

[23] I. Barin, O. Knacke, O. Kubaschewski, Thermochemical Properties of Inorganic Substances, Springer Berlin Heidelberg, Berlin, Heidelberg, 1977.

[24] W.-S. Jung, Mater. Lett. 57 (2002) 110–114.

[25] A.-H. Lu, F. Schüth, Adv. Mater. 18 (2006) 1793–1805.

[26] S.N. Talapaneni, D. Park, J. Choy, K. Ramadass, A. Elzatahry, A.S. Al Balawi, A.M. Al-

Enizi, T. Mori, A. Vinu, Chem. Sel. 1 (2016) 6062–6068.

[27] S. Geller, J. Chem. Phys. 33 (1960) 676–684.

[28] E. Auer, A. Lugstein, S. Löffler, Y.J. Hyun, W. Brezna, E. Bertagnolli, P. Pongratz, Nanotechnology 20 (2009) 434017.

[29] P. Ravadgar, R.-H. Horng, S.-D. Yao, H.-Y. Lee, B.-R. Wu, S.-L. Ou, L.-W. Tu, Appl. Phys. Lett 67 (1995) 2914–2919.

[30] B. Xu, B. Zheng, W. Hua, Y. Yue, Z. Gao, J. Catal. 239 (2006) 470–477.

[31] C. Guizani, F.J. Escudero Sanz, S. Salvador, Comptes Rendus Chim. 19 (2016) 423–432.

[32] D. Gerceker, A.H. Motagamwala, K.R. Rivera-Dones, J.B. Miller, G.W. Huber, M. Mavrikakis, J.A. Dumesic, ACS Catal. 7 (2017) 2088–2100.

[33] K. Dutta, M. Shahryari, J. Kopyscinski, Ind. Eng. Chem. Res. (2019) In-print.

[34] N. Kosinov, E.A. Uslamin, F.J.A.G. Coumans, A.S.G. Wijpkema, R.Y. Rohling, E.J.M. Hensen, ACS Catal. 8 (2018) 8459–8467.

[35] N. Kosinov, A.S.G. Wijpkema, E. Uslamin, R. Rohling, F.J.A.G. Coumans, B. Mezari, A. Parastaev, A.S. Poryvaev, M. V. Fedin, E.A. Pidko, E.J.M. Hensen, Angew. Chemie Int. Ed. 57 (2018) 1016–1020.

[36] J. Van Doorn, J.A. Moulijn, Catal. Today 7 (1990) 257–266.

[37] M. Huo, L. Li, X. Zhao, Y. Zhang, J. Li, J. Fuel Chem. Technol. 45 (2017) 172–181.

[38] N. Chino, T. Okubo, Microporous Mesoporous Mater. 87 (2005) 15–22.

List of Figures

Fig. 1. Results for nitridation of unsupported catalysts. (A) H_2O signal as a function of nitridation time at different temperatures, (B) Conversion of Ga_2O_3 as a function of temperature (C), XRD pattern as a function of temperature. (D) H_2O signal as function of nitridation time at 750 °C, (E) Conversion of Ga_2O_3 as a function of nitridation time at 750 °C and (F) XRD pattern as a function of nitridation time at 750 °C.

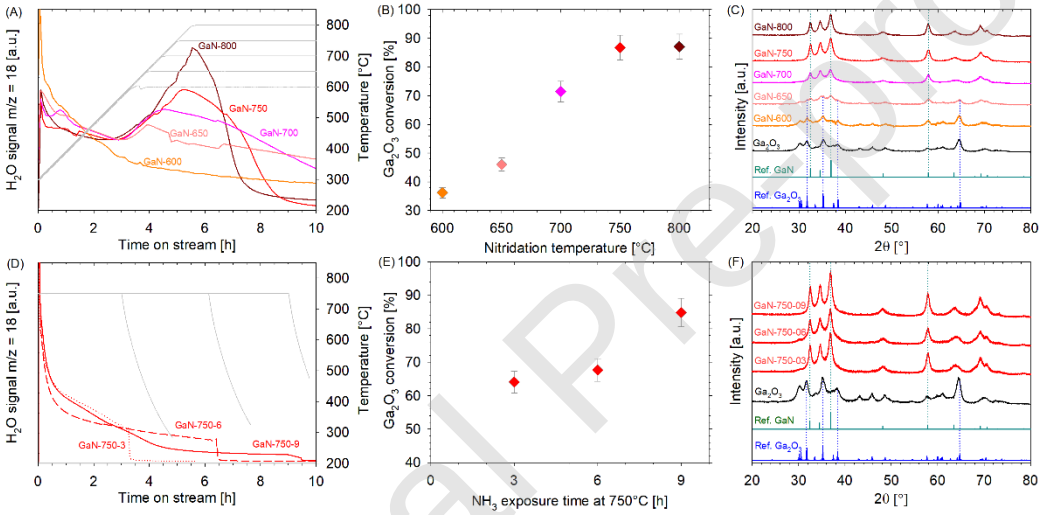

Fig. 2. HRTEM image of (A) fresh Ga_2O_3 and (B) fresh GaN-650 catalyst with GaN/Ga_2O_3 intersection. Top left inset darkfield image at low resolution and top right inset electron diffraction pattern. (C) EDS analyses (Ga normalized) for Ga_2O_3, fresh, and used GaN-650. Note: The green dashed line indicates approximately the boundary between GaN and Ga_2O_3. Note: Cu and some of the C signals in EDS are from the grid.

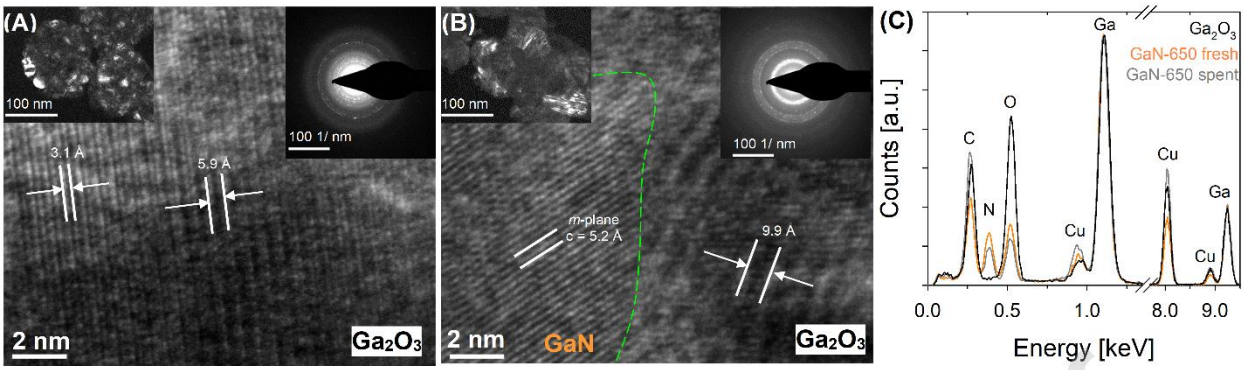

Fig. 3. Results for nitridation of supported catalysts. (A) H_2O signal and (B) XRD pattern as a function of nitridation temperature.

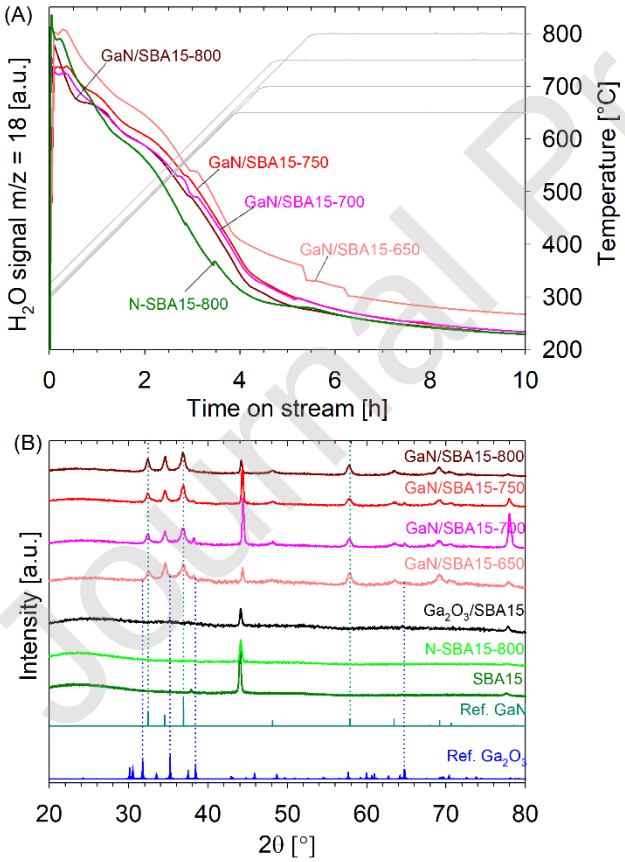

Fig. 4. STEM image of (A) fresh Ga_2O_3/SBA15 and (B) fresh GaN/SBA15-650 catalyst. Top left inset HRTEM image and top right inset electron diffraction pattern. (C) fresh GaN/SBA15-800 catalyst. Top left inset HRTEM image and top right inset electron diffraction pattern. (D) Si normalized EDS analyses for Ga_2O_3/SBA15, fresh, and used GaN/SBA15-650. Note: Cu and some of the C signals in EDS are from the grid.

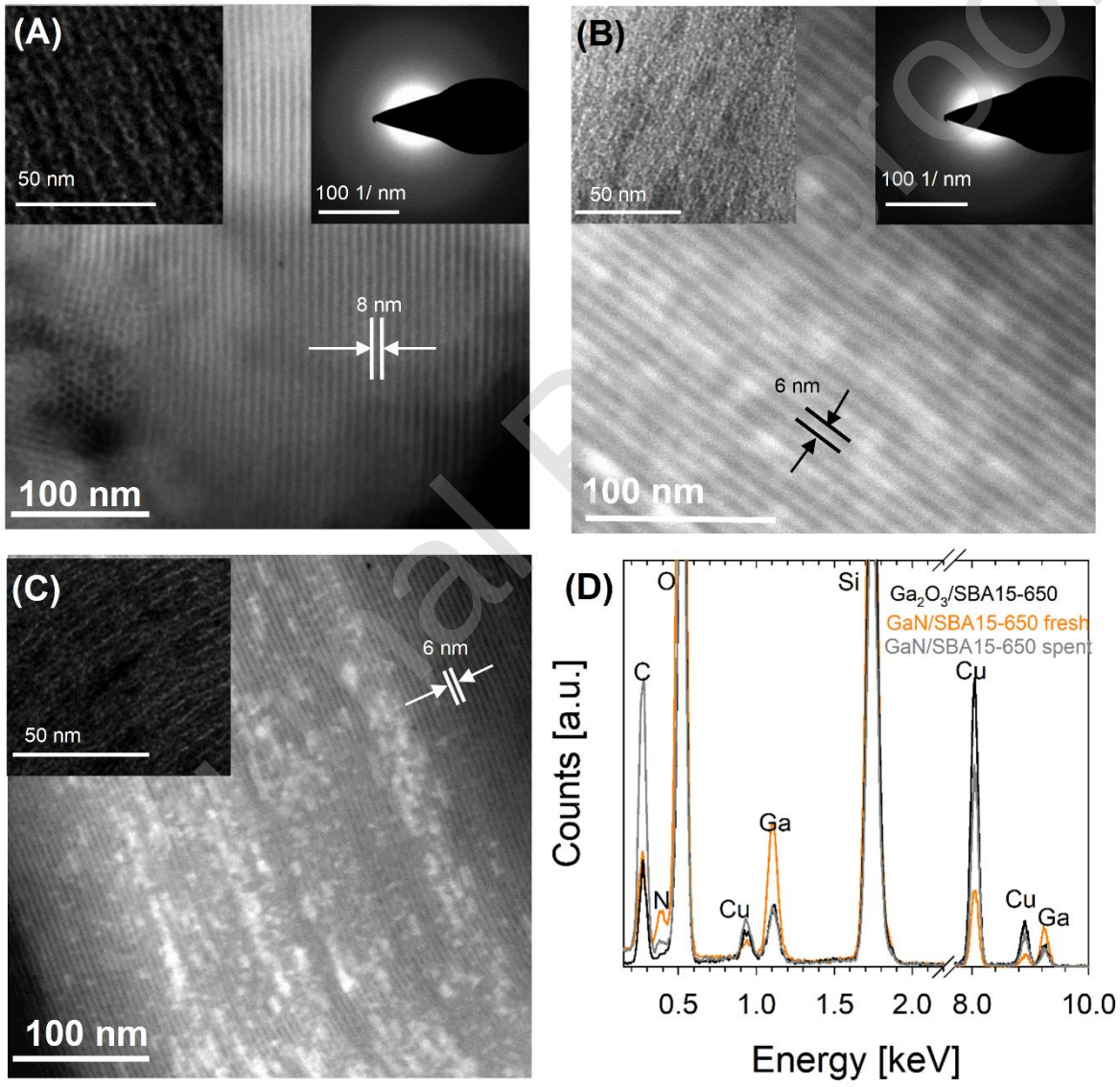

Fig. 5. Normalized mass spectra as function of time for Ga_2O_3 (A to D) and GaN-750 (E to H) for mass to charge ratios of m/z = 2 (H_2, red), m/z = 18 (H_2O, blue), m/z = 28 (C_2H_4 + CO, orange) and m/z = 44 (CO_2, grey).

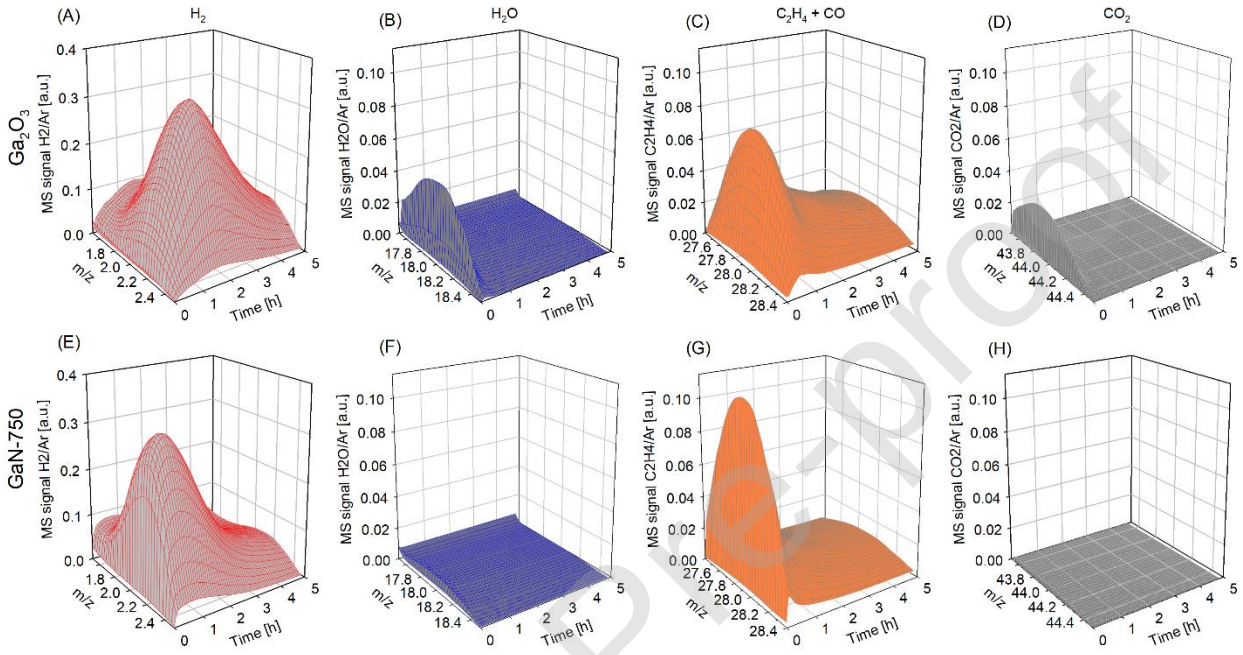

Fig. 6. (A) Methane conversion and product flow rates of (B) hydrogen, (C) ethylene (D) propylene (E) benzene and (F) toluene as a function of time on stream for the methane activation at 700 °C and 1 bar over unsupported Ga_2O_3 and GaN catalysts nitridated at different temperatures.

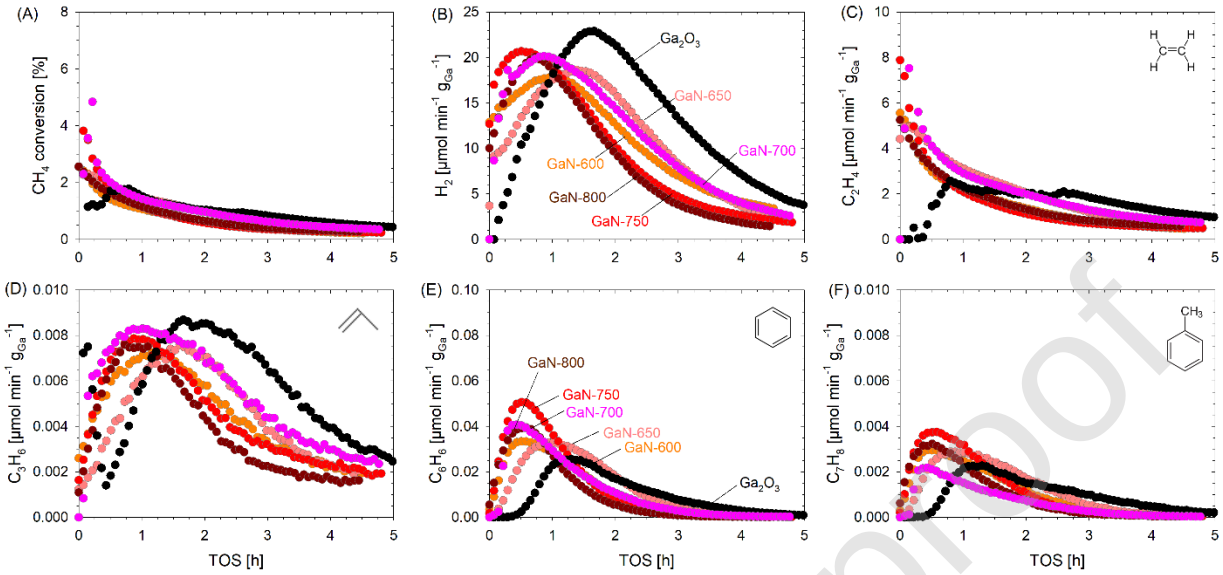

Fig. 7. (A) Methane conversion and product flow rates of (B) hydrogen (C) ethylene (D) propylene (E) benzene and (F) toluene as a function of time on stream for methane activation carried out using unsupported GaN catalysts nitridated at 750 °C at different ammonia exposure times (B). Methane activation conditions: 700 °C and 1 bar.

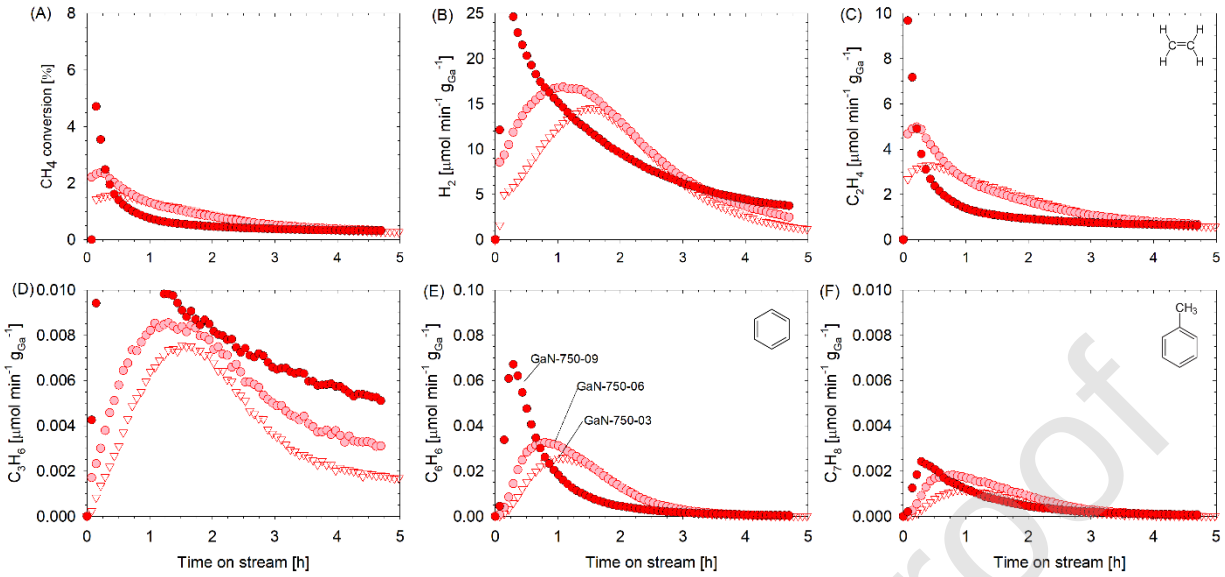

Fig. 8. TPO for spent unsupported GaN and Ga_2O_3 catalysts used for methane activation at 700 °C.

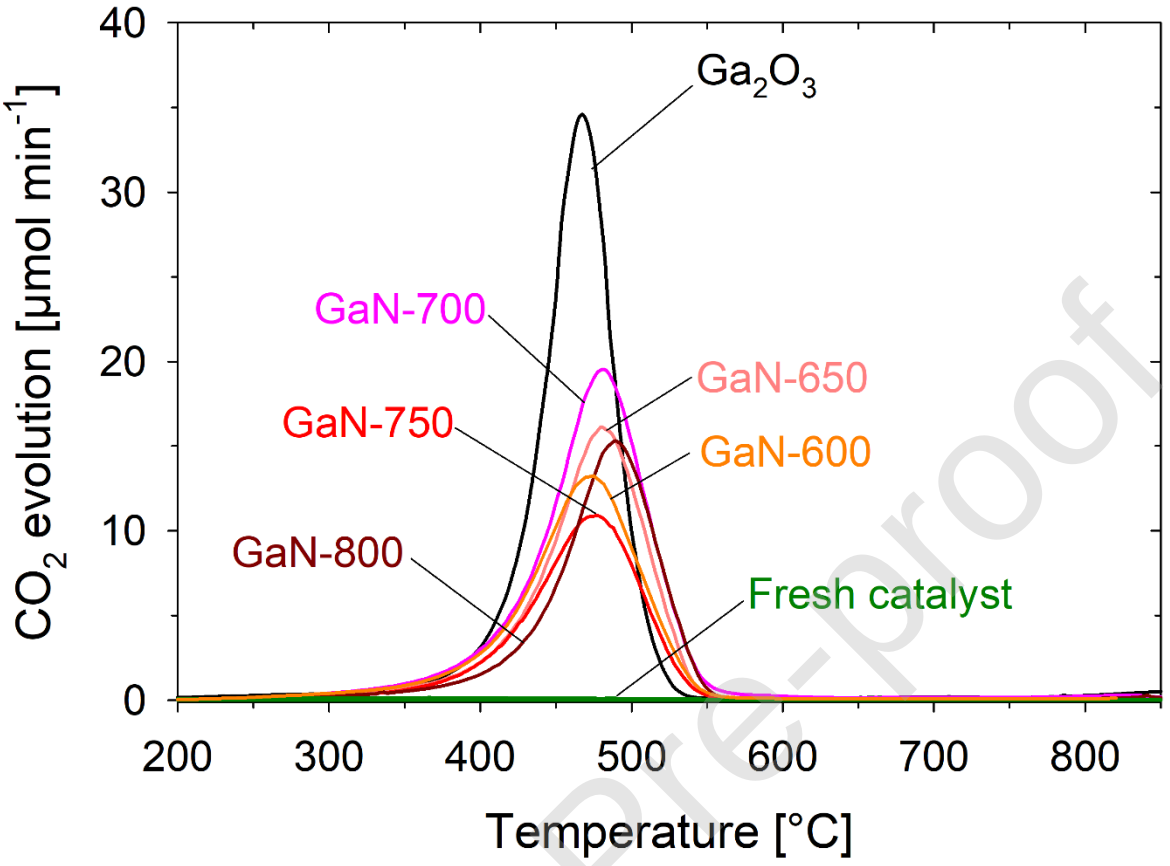

Fig. 9. Normalized mass spectra as function of time for Ga_2O_3/SBA15 (A to D), and GaN/SBA15-750 (E to H) for mass to charge ratios of m/z = 2 (H_2, red), m/z = 18 (H_2O, blue), m/z = 28 (C_2H_4 + CO, orange) and m/z = 44 (CO_2, grey).

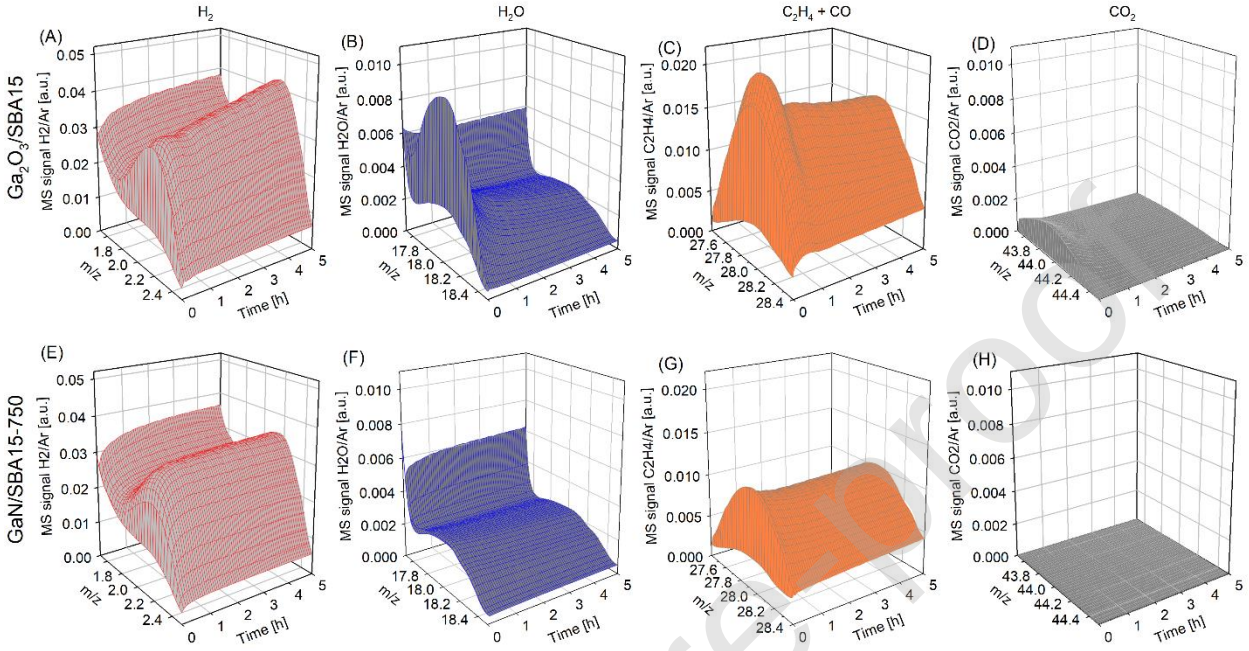

Fig. 10. (A) Methane conversion and product flow rates of (B) hydrogen, (C) ethylene, (D) propylene, (E) benzene, and (F) toluene formation rates as a function of time on stream over supported Ga_2O_3 and GaN catalyst at different nitridation temperatures. Methane activation conditions: 700 °C and 1 bar.

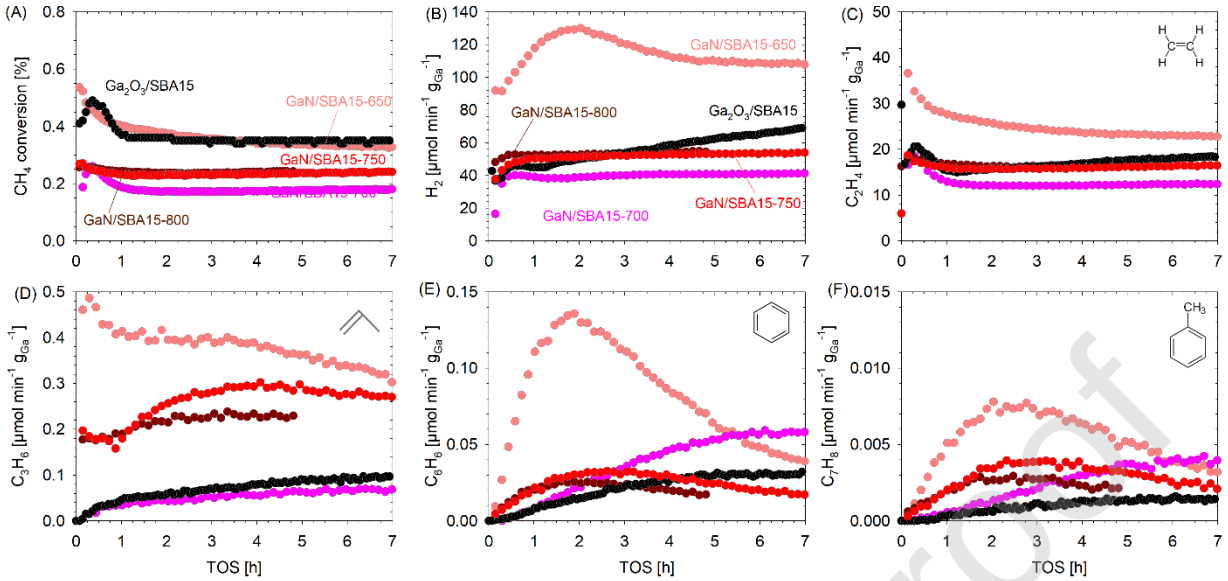

Fig. 11. TPO for spent supported GaN/Ga_2O_3 on SBA-15 catalyst used for methane activation at 700 °C.

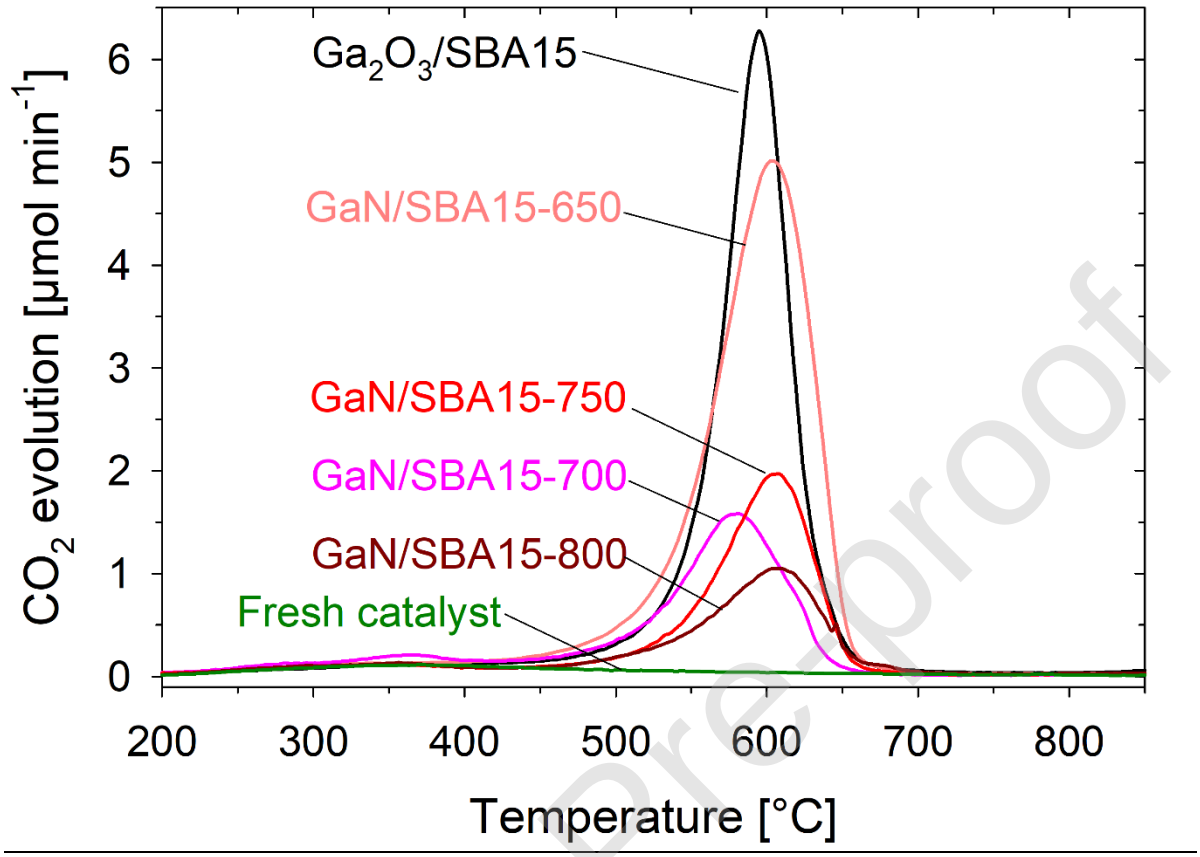

Fig. 12. Proposed underlying mechanism for methane dehydrogenation to ethylene over (A) GaN and (B) Ga_2O_3.

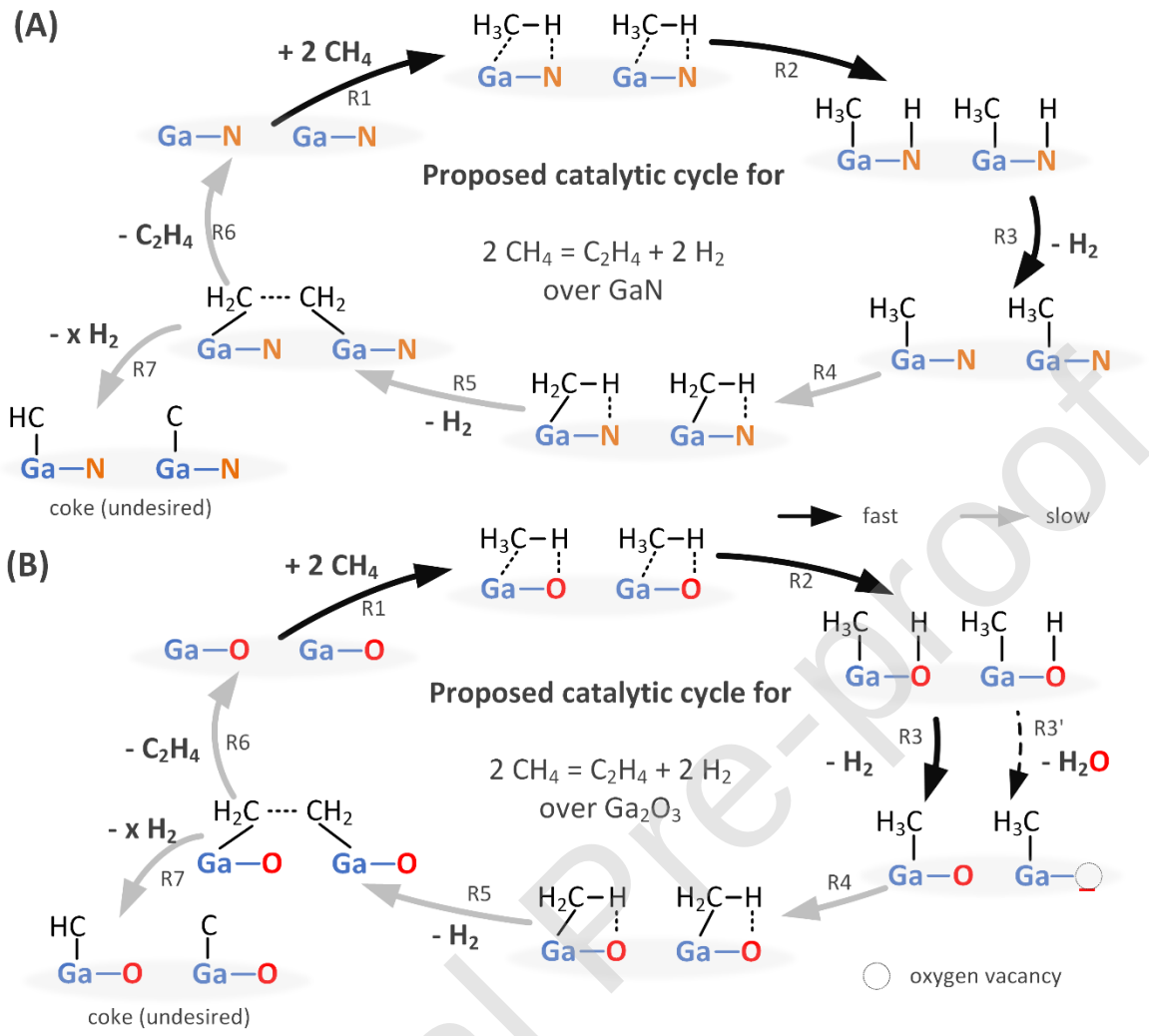

Fig. 13. Effect of nitridation on ethylene selectivity ($S_{C_2H_4}$) and adsorbed carbon (C_{ads}) on (A) unsupported GaN and (B) supported GaN/SBA15 catalysts. The dotted lines are for guidance only.

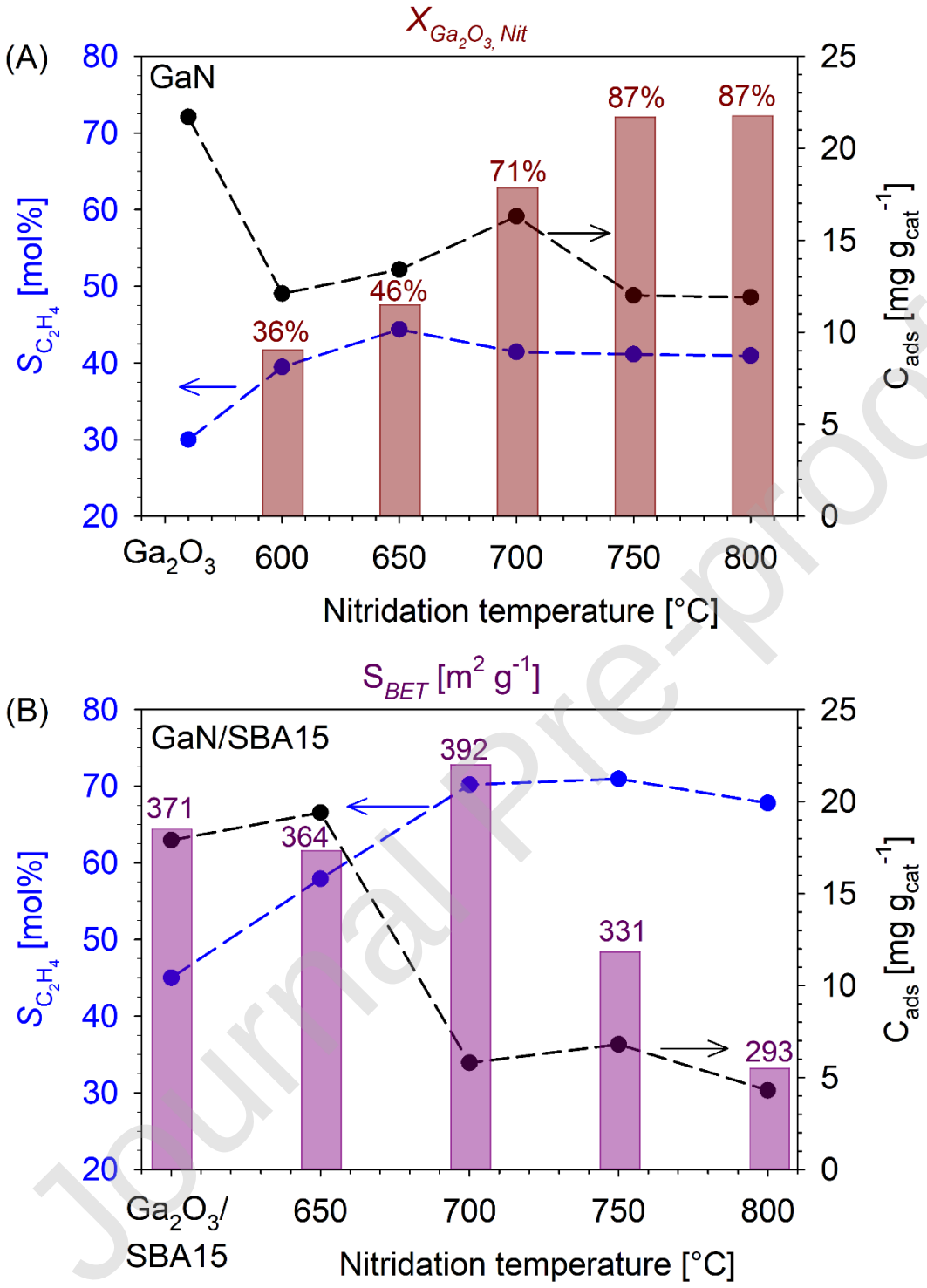

Revised manuscript No.: APCATA-D-19-02293R1

List of Tables

Table 1. Nitrogen adsorption and desorption results for unsupported Ga_2O_3, GaN catalysts.

Sample	$t_{Nitridation}$ [h]	$T_{Nitridation}$ [°C]	S_{BET} [a] [$m^2\ g^{-1}$]	S_{Micro} [a] [$m^2\ g^{-1}$]	$S_{Meso+Macro}$ [a] [$m^2\ g^{-1}$]	V_{Pore} [b] [$cm^3\ g^{-1}$]	D_{Pore} [c] [nm]
Ga_2O_3	-	-	18.9	0.8	18.1	0.083	7.5, 31.5
GaN-650	24	650	15.4	1.7	13.7	0.075	9.2, 23.1
GaN-750	24	750	11.6	1.0	10.6	0.060	9.2, 22.9
GaN-800	24	800	11.3	1.2	10.1	0.064	9.1, 29.9
GaN-750-03	3	750	14.5	1.8	12.7	0.067	9.1, 31.2
GaN-750-06	6	750	15.5	1.9	13.6	0.065	9.2, 23.6
GaN-750-09	9	750	13.4	1.4	12.0	0.069	9.2, 31.0

[a] S_{BET} = BET total specific surface area obtained from adsorption data in the p/p^0 range from 0.06-0.2; all reported data are within ± 4 $m^2\ g^{-1}$ based on repeated analysis. S_{Micro} = micropore; $S_{Meso+Macro}$= meso + macropore surface areas.

[b] V_{Pore} = pore volume was obtained at p/p^0 = 0.9

[c] D_{Pore} = bimodal pore size distribution for all samples, calculated using the Barrett-Joyner-Halenda (BJH) method;

Table 2. Nitrogen adsorption and desorption results for supported Ga_2O_3, GaN catalysts on SBA-15 (NH_3 exposure time: 24 h).

Sample	$T_{Nitridation}$ [°C]	S_{BET} [a] [$m^2\ g^{-1}$]	S_{Micro} [a] [$m^2\ g^{-1}$]	$S_{Meso+Macro}$ [a] [$m^2\ g^{-1}$]	V_{Pore} [b] [$cm^3\ g^{-1}$]	D_{Pore} [c] [nm]
SBA15	-	912	195	717	0.89	7.9
N-SBA15	800	420	61	359	0.61	8.0
Ga_2O_3/SBA15	-	426	55	371	0.53	7.9
GaN/SBA15-650	650	405	41	364	0.54	6.4
GaN/SBA15-700	700	436	44	392	0.49	6.4
GaN/SBA15-750	750	361	29	331	0.48	6.4
GaN/SBA15-800	800	320	27	293	0.44	6.3

[a] S_{BET} = BET total specific surface area obtained from adsorption data in the p/p^0 range from 0.05-0.2; all reported data are within ± 20 $m^2\ g^{-1}$ based on repeated analysis. S_{Micro} = micropore; $S_{Meso+Macro}$= meso + macropore surface areas.

[b] V_{Pore} = pore volume was obtained at p/p^0 = 0.9

[c] D_{Pore} = Unimodal pore size distribution for all samples, calculated using the Barrett-Joyner-Halenda (BJH) method;

Table 3. Overall and hydrocarbon (HC) selectivity, CH_4 conversion and C_2H_4 yield for unsupported catalysts.

Catalyst	Overall selectivity [mol%]								X_{CH4} [%][a]	Yield [%][a]
	C_2H_4	C_3H_6	C_6H_6	C_7H_8	$C_{10}H_8$	CO_2	CO	C_{ads}[b]	CH_4	C_2H_4
Ga_2O_3	27-34	0.13	0.46	0.06	0.01	1.2	0-7	65.09	2.7-2.9	0.7-1.1
GaN-600	39.46	0.17	0.88	0.10	0.02	-	-	59.37	1.80	0.71
GaN-650	44.38	0.14	0.83	0.09	0.02	-	-	54.53	2.18	0.97
GaN-700	41.44	0.16	0.68	0.05	0.02	-	-	57.66	2.46	1.02
GaN-750	41.12	0.83	1.08	0.12	0.02	-	-	57.47	1.75	0.72
GaN-800	40.96	0.15	0.84	0.09	0.02	-	-	57.94	1.87	0.76
GaN-750-03	49.11	0.18	0.76	0.04	0.02	-	-	49.88	1.55	0.76
GaN-750-06	38.17	0.17	0.70	0.05	0.02	-	-	60.87	2.29	0.87
GaN-750-09	30.78	0.27	0.74	0.05	0.02	-	-	68.12	2.13	0.66

[a] based on total products [mol] determined by integration of molar flow rates vs. time on stream (5 h)
[b] adsorbed carbon based on TPO = temperature-programmed oxidation

Table 4. Overall and hydrocarbon selectivity for supported catalysts.

Catalyst	Overall selectivity [mol%]								X_{CH4} [%][a]	Yield [%][a]
	C_2H_4	C_3H_6	C_6H_6	C_7H_8	$C_{10}H_8$	CO_2	CO	C_{ads}[b]	CH_4	C_2H_4
Ga_2O_3/SBA15	43−58	0.30	0.01	0.18	0.01	1.7	0−15	39.71	0.6−0.7	0.25−0.45
GaN/SBA15-650	57.91	1.32	0.57	0.04	0.02	-	-	40.14	0.60	0.35
GaN/SBA15-700	70.18	0.42	0.60	0.05	0.01	-	-	28.74	0.26	0.18
GaN/SBA15-750	70.94	1.70	0.30	0.04	0.02	-	-	26.98	0.32	0.23

GaN/SBA15-800	67.79	1.71	0.33	0.04	0.01	-	-	30.09	0.26	0.18

[a] based on total products [mol] determined by integration of molar flow rates vs. time on stream (7 h)
[b] adsorbed carbon based on TPO = temperature-programmed oxidation